Atmos. Chem. Phys., 12, 8727–8750, 2012
www.atmos-chem-phys.net/12/8727/2012/
doi:10.5194/acp-12-8727-2012
© Author(s) 2012. CC Attribution 3.0 License.

Atmospheric Chemistry and Physics

Impact of forest fires, biogenic emissions and high temperatures on the elevated Eastern Mediterranean ozone levels during the hot summer of 2007

Ø. Hodnebrog[1,2], S. Solberg[3], F. Stordal[1], T. M. Svendby[3], D. Simpson[4,5], M. Gauss[4], A. Hilboll[6], G. G. Pfister[7], S. Turquety[8], A. Richter[6], J. P. Burrows[6], and H. A. C. Denier van der Gon[9]

[1]Department of Geosciences, University of Oslo, Norway
[2]Center for International Climate and Environmental Research-Oslo (CICERO), Norway
[3]Norwegian Institute for Air Research, Kjeller, Norway
[4]Norwegian Meteorological Institute, Oslo, Norway
[5]Dept. Earth & Space Sciences, Chalmers University of Technology, Göteborg, Sweden
[6]Institute of Environmental Physics, University of Bremen, Germany
[7]Atmospheric Chemistry Division, National Center for Atmospheric Research, Boulder, CO, USA
[8]Laboratoire de Météorologie Dynamique/IPSL, UPMC Univ. Paris 06, Paris, France
[9]TNO, Business unit Environment, Health and Safety, Utrecht, The Netherlands

Correspondence to: Ø. Hodnebrog (oivind.hodnebrog@cicero.uio.no)

Received: 14 November 2011 – Published in Atmos. Chem. Phys. Discuss.: 16 March 2012
Revised: 6 September 2012 – Accepted: 13 September 2012 – Published: 27 September 2012

Abstract. The hot summer of 2007 in southeast Europe has been studied using two regional atmospheric chemistry models; WRF-Chem and EMEP MSC-W. The region was struck by three heat waves and a number of forest fire episodes, greatly affecting air pollution levels. We have focused on ozone and its precursors using state-of-the-art inventories for anthropogenic, biogenic and forest fire emissions. The models have been evaluated against measurement data, and processes leading to ozone formation have been quantified. Heat wave episodes are projected to occur more frequently in a future climate, and therefore this study also makes a contribution to climate change impact research.

The plume from the Greek forest fires in August 2007 is clearly seen in satellite observations of CO and NO_2 columns, showing extreme levels of CO in and downwind of the fires. Model simulations reflect the location and influence of the fires relatively well, but the modelled magnitude of CO in the plume core is too low. Most likely, this is caused by underestimation of CO in the emission inventories, suggesting that the CO/NO_x ratios of fire emissions should be re-assessed. Moreover, higher maximum values are seen in WRF-Chem than in EMEP MSC-W, presumably due to differences in plume rise altitudes as the first model emits a larger fraction of the fire emissions in the lowermost model layer. The model results are also in fairly good agreement with surface ozone measurements.

Biogenic VOC emissions reacting with anthropogenic NO_x emissions are calculated to contribute significantly to the levels of ozone in the region, but the magnitude and geographical distribution depend strongly on the model and biogenic emission module used. During the July and August heat waves, ozone levels increased substantially due to a combination of forest fire emissions and the effect of high temperatures. We found that the largest temperature impact on ozone was through the temperature dependence of the biogenic emissions, closely followed by the effect of reduced dry deposition caused by closing of the plants' stomata at very high temperatures. The impact of high temperatures on the ozone chemistry was much lower. The results suggest that forest fire emissions, and the temperature effect on biogenic emissions and dry deposition, will potentially lead to substantial ozone increases in a warmer climate.

Published by Copernicus Publications on behalf of the European Geosciences Union.

1 Introduction

Three distinct heat waves and associated forest fire events led to elevated ozone (O_3) and particulate matter (PM) levels in the Eastern Mediterranean region during the summer of 2007 (Eremenko et al., 2008; Liu et al., 2009). The Greek forest fires were the most extensive and destructive in the recent history of the country, and they were a consequence of several heat waves and long periods of drought (Founda and Giannakopoulos, 2009). In fact, several stations in Greece reported record breaking temperatures (up to 47 °C), making this the hottest summer on record. In Greece, more than 12 % of the forested area burnt (Kaskaoutis et al., 2011), contributing substantially to the air pollution levels in Athens (Liu et al., 2009). Extreme levels of carbon monoxide (CO) were observed from satellites, indicating up to 22 ppmv close to the fires and 4 ppmv in the plume transported above the Mediterranean basin (Turquety et al., 2009).

Ozone is formed from photochemical reactions, following emissions of the ozone precursors CO, nitrogen oxides (NO_x) and Non-Methane Volatile Organic Compounds (NMVOC) (e.g. Crutzen, 1974; Atkinson, 2000), and is also strongly affected by meteorological conditions (e.g. Jacob and Winner, 2009). In particular, temperature has a large impact on ozone and substantial increases in surface ozone have previously been documented during heat wave episodes, e.g. during the European heat wave in the summer of 2003 (Vautard et al., 2005; Solberg et al., 2008). The impacts of temperature on atmospheric ozone occur both directly through the temperature dependence of ozone forming reactions (Sillman and Samson, 1995), and indirectly through the temperature dependence of dry deposition through stomatal uptake (e.g. Wesely, 1989; Solberg et al., 2008) and biogenic emissions of ozone precursors (e.g. Guenther et al., 1993), all of which favours ozone formation when temperatures increase. Additional meteorological factors associated with heat waves, causing higher ozone, include: increased solar radiation leading to both more intense photochemistry and enhanced biogenic emissions, high-pressure areas leading to stagnant conditions and thereby less ventilation of air pollution in the boundary layer, and lower soil moisture causing the plants' stomata to close and thereby reducing the biogenic uptake. An exception from these positive ozone responses is that dryer air leads to less formation of the OH radical and thereby slower oxidation of the NMVOCs, the "fuel" in the ozone formation.

The Eastern Mediterranean basin is constantly exposed to air pollution from the surrounding densely populated areas (Kanakidou et al., 2011). Furthermore, the region is presently experiencing a rapid urbanization. Maximum ozone mixing ratios in and downwind of major urban areas in Greece are found to exceed the European Union (EU) health risk threshold level of 180 $\mu g\,m^{-3}$ during summer (Poupkou et al., 2009), and in large parts of the Eastern Mediterranean region ozone concentrations throughout the year exceed levels known to cause vegetation damages (Kourtidis et al., 2002). The region acts as a reservoir for anthropogenic pollutants originating from the nearby emission hotspots Cairo, Istanbul and Athens, from maritime transport emissions (Poupkou et al., 2008), and from more distant sources, particularly the European continent (Lelieveld et al., 2002; Gerasopoulos et al., 2005). Additionally, biogenic emissions of isoprene, monoterpenes and other VOCs are large on the Balkan Peninsula, and represent 70–80 % of the annual total NMVOC emissions in most of the countries in this region (Symeonidis et al., 2008). Considering that isoprene is about a factor of three more photochemically reactive than a weighted average of VOCs emitted by e.g. motor vehicle exhaust (Benjamin et al., 1997), the potential impact of biogenic emissions on air pollution is strong. Ozone formation is also favoured by the meteorological conditions typical of the Mediterranean climate; strong insolation, high temperatures, and a low number of precipitation days. Results from regional climate models indicate that heat waves may occur more frequently in the future (Beniston, 2004; Schär et al., 2004), and that the maximum daily temperatures observed over southeastern Europe during the exceptionally hot and dry summer of 2007 may be more frequent in the latter half of the 21st century (Founda and Giannakopoulos, 2009). Such conditions also imply an increased risk of forest fires, which would further increase future air pollution levels.

Several studies have investigated gas-phase and particle pollution in Southern Europe, both by observation analysis and by the use of atmospheric chemistry models (e.g. Millan et al., 2000, 2002; Andreani-Aksoyoglu et al., 2004; Lazaridis et al., 2005; Calori et al., 2008; Astitha and Kallos, 2009; Curci et al., 2009; Schürmann et al., 2009; Im and Kanakidou, 2012). Many of these studies have highlighted the role of local and regional meteorological characteristics on air pollution in this region, e.g. sea-breeze circulation in the Athens area (Melas et al., 1998), the etesian winds in the Aegean sea (Kallos et al., 1993), recirculations induced by the mountains surrounding the Mediterranean basin (Millan et al., 1997), and long-range transport patterns of air pollutants to and from the Mediterranean region (Kallos et al., 2007, and references therein). In a model study by Baertsch-Ritter et al. (2004) a strong dependence of temperature on net ozone formation was found in Northern Italy with 2.8 ppb O_3 K^{-1} for a high ozone episode in Milan, while the impact on ozone levels due to changes in humidity was relatively small. The impact of temperature changes on ozone in the Eastern Mediterranean was recently studied by Im et al. (2011a). They found an almost linear ozone increase with temperature of 0.9 ± 0.1 ppb O_3 K^{-1}, and a temperature-induced increase in biogenic isoprene emissions of 9 ± 3 % K^{-1}. Both Vieno et al. (2010) and Solberg et al. (2008) highlighted the role of surface dry deposition during the European summer 2003 heat wave, indicating that reduced uptake from vegetation due to drought contributed significantly to high ozone levels. Furthermore, biogenic isoprene emissions contributed

up to 20 % of the peak ozone values, and a 10 K increase led to a 5 % increase in peak ozone (Solberg et al., 2008).

The present study was carried out as part of the EU FP7 project CityZen, which aimed at determining the air pollution distribution and change in and around emission hotspots in Europe and Asia. It also builds upon emission data developed in its EU FP7 sister project MEGAPOLI. The Eastern Mediterranean, which is the focus here, was one of the selected hotspots within the CityZen project and the extreme summer 2007 was selected as a case study. This study aims at quantifying the influences of various processes on the elevated ozone levels in the Eastern Mediterranean during summer 2007. Several simulations have been conducted for this purpose, using two regional atmospheric chemistry models. Descriptions of the model tools, emissions and simulation setups are given in Sect. 2, while the results including comparisons with observations are presented and discussed in Sect. 3. Finally, our conclusions are given in Sect. 4.

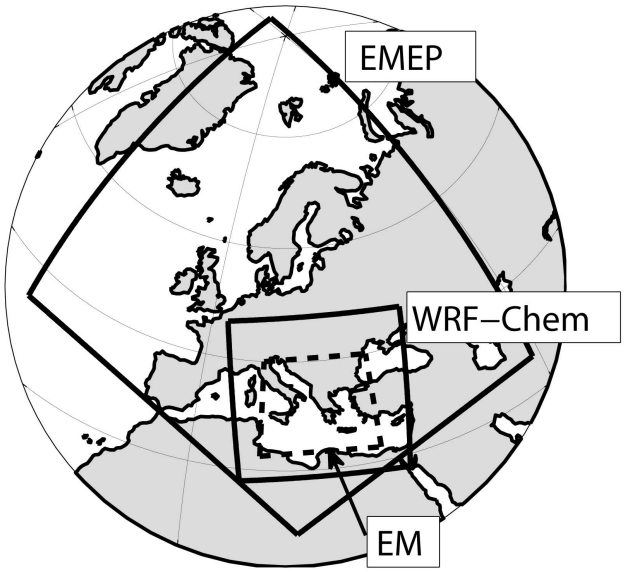

Fig. 1. Locations of the domains used in the EMEP MSC-W and WRF-Chem simulations, and of the study region (11–30° E, 32–45° N) covering most of the Eastern Mediterranean (EM). Coordinates of the four corners of the two model domains are (35.8° W, 40.5° N), (16.7° E, 20.3° N), (58.6° E, 34.8° N) and (131.8° W, 86.5° N) for EMEP MSC-W, and (8.1° E, 28.2° N), (33.9° E, 28.2° N), (38.8° E, 49.8° N) and (3.2° E, 49.8° N) for WRF-Chem.

2 Models and methodology

Two regional atmospheric chemistry models were applied; the Weather Research and Forecasting model with Chemistry (WRF-Chem) (Grell et al., 2005) and EMEP MSC-W (Simpson et al., 2012). Both models used a horizontal resolution of 25 km × 25 km, and have been run for three summer months of 2007; June, July and August (plus two weeks of spin-up in May). The WRF-Chem model domain is centred over the Balkan Peninsula, covers most of the Mediterranean sea in the south, and extends up to mid-Germany in the north, while the EMEP model domain is much larger, covering all of Europe (Fig. 1). In order to simplify the presentation of results, a common domain has been defined, which covers the region of most interest in the Eastern Mediterranean (hereafter denoted EM), and which is well within the domain borders of both models. A comparison of the model properties and setups is given in Table 1, while brief descriptions of each of the models are given below.

2.1 WRF-Chem model

The WRF-Chem model (Grell et al., 2005) consists of a mesoscale meteorological model (WRF) (Skamarock and Klemp, 2008) coupled with a chemistry module. In this study, WRF-Chem version 3.2 has been used with the RADM2 gas-phase chemistry scheme (Stockwell et al., 1990). The modules and meteorological physics schemes are the same as in Hodnebrog et al. (2011), but the following modification has been applied to the FTUV (Madronich, 1987) photolysis scheme. Instead of a fixed overhead ozone column amount, the model uses a domain-averaged total O_3 column value in the calculation of photolysis rates for each day of the simulation. The overhead ozone column is calculated by the global Oslo CTM2 model (Søvde et al., 2008) using a simulation setup described in the Supplement, Table A1. Of particular interest in this study is dry convection, which is included in the Grell-3 cumulus scheme adopted here. Meteorological initial and boundary conditions are taken from ECMWF-IFS model analysis at a resolution of 0.25° × 0.25° and updated every 6 h (http://www.ecmwf.int/research/ifsdocs/). Furthermore, the meteorological parameters temperature, humidity and horizontal winds calculated by WRF are nudged towards the ECMWF-IFS data every time step. Initial and boundary conditions for the chemical species are updated every 6 h from results obtained with the Oslo CTM2 model, which also uses meteorological data from ECMWF-IFS. As the Oslo CTM2 and RADM2 chemistry schemes differ, the NMVOC species in the Oslo CTM2 model had to be mapped to the appropriate RADM2 components. The calculation of biogenic emissions is done online using the Model of Emissions of Gases and Aerosols from Nature (MEGAN) version 2.04 (Guenther et al., 2006), and the calculation of dry deposition uses the Wesely (1989) scheme. In estimation of the stomata resistance in the Wesely parameterization only the temperature and the incoming solar radiation are taken into account. The uptake of ozone is optimal near 20 °C and reduced for higher and lower temperatures, whereas it increases monotonically with increasing incoming solar radiation. Thus moisture in the atmosphere and the soil, which are known to impact on the stomata opening, are neglected in the calculations of the

Table 1. Setups of the participating models; WRF-Chem and EMEP.

Model	WRF-Chem v. 3.2	EMEP MSC-W rv. 3.7.7
Operated by	Univ. of Oslo	NILU
Developed by	NOAA/NCAR and others	Met.no
Model type	Regional NWP + CTM	Regional CTM
Horizontal resolution	25 km × 25 km	25 km × 25 km
Horizontal grid size	104 × 99	264 × 318
Number of vertical levels	27	20
Height of lowermost level	∼ 58 m	∼ 90 m
Model top	50 hPa	100 hPa
Meteorology	WRF (coupled w/chemistry)	HIRLAM (interp. from 10 km × 10 km)
Meteorological initial and boundary conditions	ECMWF-IFS*	ECMWF-IFS*
Chemistry scheme	RADM2 (Stockwell et al., 1990)	EMEP (Simpson et al., 2012)
Chemical initial and boundary conditions	Oslo CTM2 (Søvde et al., 2008)	Climatological, based upon measurements and ozone-sondes, see Simpson et al. (2012)
Chemical species	63	71
Chemical reactions	158	140
Anthropogenic emissions	TNO-MACC (Kuenen et al., 2011)	Redistributed EMEP (http://www.ceip.at; Visschedijk et al., 2007)
Biomass burning emissions	FINNv1 (Wiedinmyer et al., 2011)/GFEDv2 (van der Werf et al., 2006)	GFEDv2 (van der Werf et al., 2006)
Biogenic emissions	MEGAN v. 2.04 (Guenther et al., 2006) online calculation	EMEP isoprene (Simpson et al., 1999) online calculation
References	Grell et al. (2005)	Simpson et al. (2012)

* Documentation can be found at http://www.ecmwf.int/research/ifsdocs/.

ozone stomata uptake and ozone dry deposition in the current WRF-Chem scheme.

2.2 EMEP MSC-W model

The EMEP MSC-W model is a chemical transport model (CTM) developed at the EMEP Meteorological Synthesizing Centre – West (EMEP MSC-W) at the Norwegian Meteorological Institute. The model is a development of the 3-D model of Berge and Jakobsen (1998), extended with photo-oxidant chemistry (Andersson-Sköld and Simpson, 1999; Simpson et al., 2012) and the version used here (rv. 3.7.7) makes use of the EQSAM gas/aerosol partitioning model (Metzger et al., 2002). Anthropogenic emissions from European ground-level sources are supplied as gridded annual fields of NO_x, NH_3, SO_2, fine and coarse particulate matter, CO, and non-methane VOC (NMVOC), modified with monthly and daily factors. The methodology for biogenic emissions used in the EMEP model has undergone a substantial update during 2011, now building upon maps of 115 forest species generated by Köble and Seufert (2001). Emission factors for each forest species and for other land-classes are based upon Simpson et al. (1999), updated with recent literature (see Simpson et al. (2012) and references therein), and driven by hourly temperature and light using algorithms from Guenther et al. (1993). Other emissions include NO_x from aircraft and lightning, marine emissions of dimethylsulphide, and SO_2 from volcanoes.

Dry deposition is calculated using a resistance analogy combined with stomatal and non-stomatal conductance algorithms (Emberson et al., 2001; Simpson et al., 2003, 2012),

whereas wet deposition uses scavenging coefficients applied to the 3-D rainfall. The model has traditionally been used at $50 \times 50\,km^2$ resolution over Europe, but is flexible with respect to input meteorological data and domain, with applications ranging from $5 \times 5\,km^2$ over the UK to $1° \times 1°$ globally (Jonson et al., 2010a, b; Vieno et al., 2010). Chemical initial and boundary conditions are from climatology and based on measurements and ozone sondes (Simpson et al., 2012). Full details of the EMEP model are given in Simpson et al. (2012).

2.3 Emissions

Emissions of the ozone precursors CO, NO_x and NMVOC have been included in the models from anthropogenic and biogenic sources, as well as emissions originating from forest fires. In both models, the anthropogenic emissions are based on the country total emissions officially reported to EMEP, but the methods used to grid the emissions to fine scale are different. In WRF-Chem we have used the TNO-MACC emission inventory (Kuenen et al., 2011), which has a resolution of 1/8° longitude × 1/16° latitude (approximately 10 km × 7 km in the EM region), and is developed within the MEGAPOLI project. Over North Africa, including Cairo, emissions from the RETRO (2006) inventory were used. Emissions from both inventories were horizontally interpolated to the model grid. Next, a splitting of the aggregated NMVOC component in the TNO-MACC inventory was made based on the UK emissions of the 50 most significant NMVOC species (Dore et al., 2007). Factors were derived for each NMVOC species and each emission sector, and then applied to each grid cell in order to obtain individual NMVOC species, which were then lumped to the RADM2 components by using the information provided in Middleton et al. (1990) and Stockwell et al. (1990). The emissions used in the EMEP model are country totals redistributed using Visschedijk et al. (2007), and are provided for 10 anthropogenic source-sectors denoted by so-called SNAP codes. The speciation of NMVOC within each SNAP sector is as given in Simpson et al. (2012). The emissions database is available from http://www.ceip.at and further details can be obtained at that site. Before implementing the anthropogenic emissions into the models, factors to account for diurnal, weekly, and monthly cycles, as well as the vertical distribution, were applied to both inventories according to Simpson et al. (2012).

Table 2 lists the emission totals used in this study, while Figs. 2 and 3 show the horizontal distribution and the time evolution, respectively, of the NO_x emissions from the various inventories for the Eastern Mediterranean region. The anthropogenic emission inventories have similar distributions, and show hotspots in Po Valley, Athens, Istanbul and Cairo, as well as fairly large emissions coming from ship traffic in the Mediterranean Sea (Fig. 2). In total, however, the anthropogenic emissions of CO, NO_x and NMVOC are higher in the TNO-MACC inventory compared to the regridded EMEP inventory (Table 2). Both emission inventories are largely based on official reported emission to EMEP but gaps are filled using expert estimates. This is relevant for a number of countries in the region of study e.g., Turkey, Serbia and Ukraine. The origin of the emission data used in the TNO-MACC emission inventory as well as the procedure to grid the emissions over the domain is described in detail by Denier van der Gon et al. (2010).

Forest fires turned out to be an important contribution to the atmospheric pollution level during the East Mediterranean heat waves in summer 2007. Thus, such emissions had to be included in the WRF-Chem and EMEP models. Forest fire emissions were taken from the Global Fire Emission Database version 2 (GFEDv2) (van der Werf et al., 2006) and from the newly developed Fire INventory from NCAR version 1 (FINNv1) (Wiedinmyer et al., 2011). The temporal and spatial resolutions differ substantially between the two inventories; the first providing $1° \times 1°$ gridded data for 8-day averages, whereas the latter provides daily emissions on $1\,km \times 1\,km$ resolution. According to Table 2, the total emissions provided by each inventory for the summer 2007 forest fires in the EM are also quite different, at least for NO_x and CO, showing higher emissions in the GFEDv2 inventory compared to FINNv1. In general, differences between FINN and GFED can vary regionally due to different assumptions of fuel inputs, emission factors, as well as in the burned area and fire identification. The higher NMVOCs in FINN is due to the fact that new emission factors and a different NMVOC speciation have been used in FINN, as discussed in Wiedinmyer et al. (2011). Figure 2 shows that the GFED NO_x emissions are higher than FINN for both the Albanian and Greek forest fire episodes, but slightly lower for the fires occurring in Italy. One of the most intense forest fire episodes took place between 20–31 July (Fig. 3), when fires broke out both at Peloponnese in Greece, and along the coast of Albania. Around 21 August, new intense fires emerged, mainly in southern Greece, and continued into early September.

Figure 4 shows that the summer 2007 was exceptional when it comes to forest fire emissions in the Eastern Mediterranean, with more than 1800 kt of CO emitted in the EM domain. Within the period of available GFEDv2 monthly data (1997–2008), the vast forest fire emissions of CO during the summer of 2007 are only exceeded by the summer of 2000.

The WRF-Chem model has been run with the FINN emissions, except for a sensitivity test with GFED. For both inventories, a diurnal profile was added according to WRAP (2005), and the WRF-Chem online plume rise routine (Freitas et al., 2007) was applied in order to vertically distribute the fire emissions. The 8-day GFEDv2 inventory (van der Werf et al., 2006) only contains gridded emissions for total NMVOCs, but not for the individual NMVOC species required for the RADM2 and EMEP MSC-W chemistries. A dataset containing individual NMVOC components has

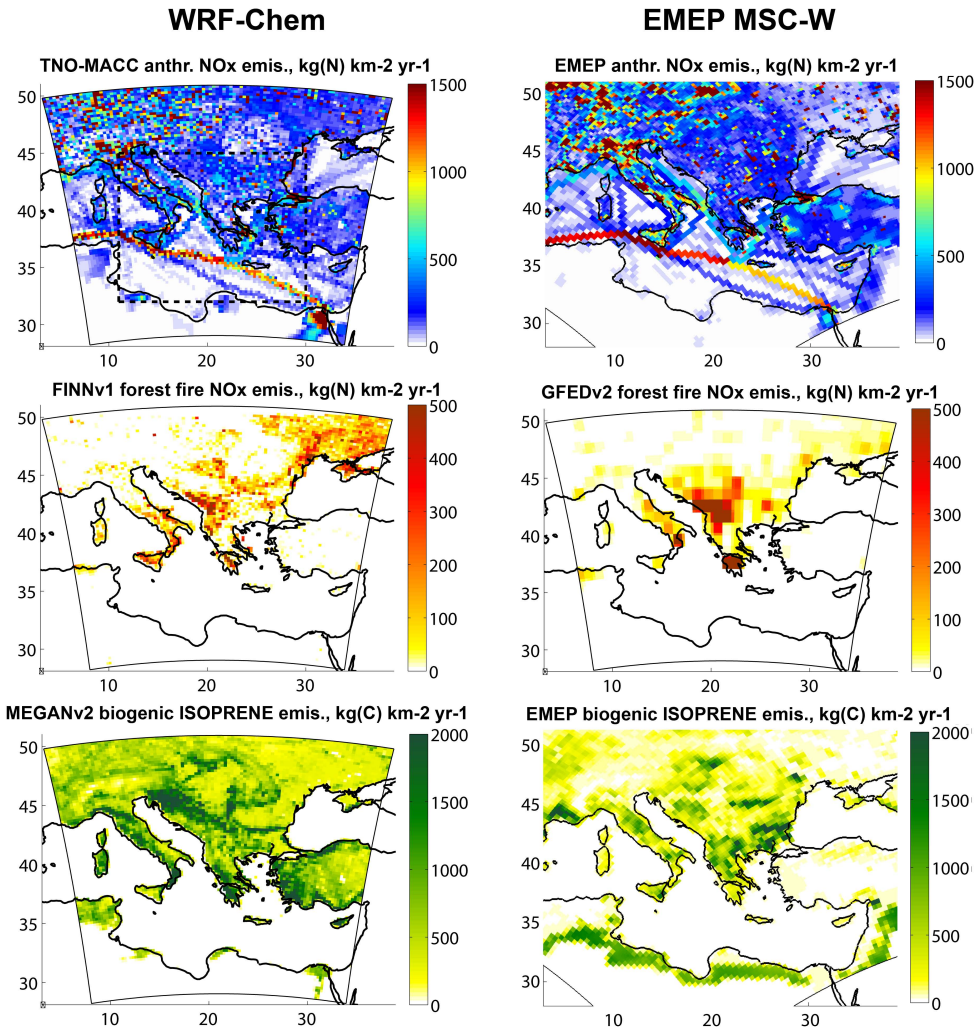

Fig. 2. Seasonally (June, July, August) averaged emissions of NO_x (kg(N) km^{-2} yr^{-1}) from anthropogenic sources (top) and forest fires (middle), and emissions of isoprene (kg(C) km^{-2} yr^{-1}) from biogenic sources (bottom) as used in the reference simulations of the WRF-Chem (left) and EMEP MSC-W (right) models. The dashed rectangle in the topleft plot marks the EM region.

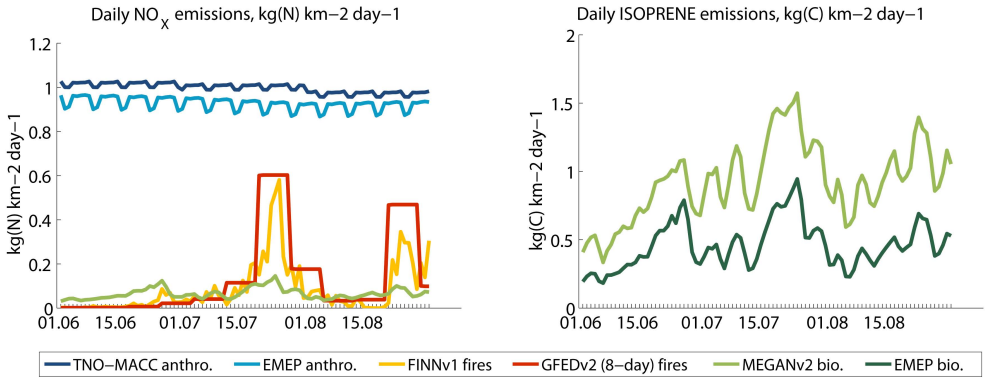

Fig. 3. Temporal evolution of NO_x emissions from various sources (left; kg(N) km^{-2} day^{-1}), and of isoprene from biogenic sources (right; kg(C) km^{-2} day^{-1}) averaged over the region marked by the dashed rectangle in Fig. 2. Biogenic soil emissions of NO are not included in the EMEP model.

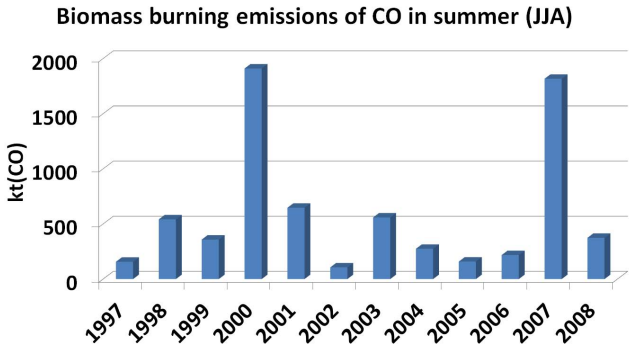

Fig. 4. Biomass burning emissions of CO (kt CO) integrated over the summer period (June, July, August) and over the region marked by the dashed rectangle in Fig. 2, as reported in the GFEDv2 emission inventory (van der Werf et al., 2006).

been provided (A. Heil, personal communication, 2011) and was calculated from the GFEDv2 dry matter burned data in combination with the GFEDv2 vegetation map and updated vegetation-type specific emission factors based on Andreae and Merlet (2001). The EMEP model version used here also makes use of the 8-daily fire emissions from GFED, for SO_2, CO, NO_x, NMHC, and particles. The emissions are homogeneously distributed over the eight lowest layers of the model (to about 1.8 km), based on recommendations by Sofiev et al. (2009) to use a PBL height as an approximate height for emission injection. For comparison, the vertical distribution of the GFED emissions calculated with the plume rise routine in WRF-Chem is very inhomogeneous. About 70 % is emitted in the lowermost layer (to about 60 m) and about 15 % above 1.8 km height, while the remaining 15 % are distributed between 60 and 1800 m.

Biogenic emissions are calculated online in both models, and depend on land-use data and weather conditions. In WRF-Chem, the MEGAN module depends on ambient temperature, photosynthetic active radiation (PAR), humidity, wind speed and soil moisture when estimating emissions of isoprene, monoterpenes, other biogenic VOCs, and nitrogen emissions from soil. In the EMEP model biogenic emissions of isoprene and monoterpenes are calculated at every model timestep using near-surface air temperature and PAR. The latter variable is in both models calculated from the solar radiation, modified by the total cloud fraction. A possible concern regarding emissions from vegetation is that the land-cover maps used to calculate biogenic emissions have no knowledge of the effects of the forest fires. Hence, in some land areas the biomass burning emissions may be added at the top of the biogenic emissions. However, we do not consider this is a large problem compared to uncertainties in forest fire and biogenic emissions in general. As shown in Table 2, there is approximately a factor of two difference in biogenic isoprene emissions when two different modules are being used.

The temporal evolution of biogenic isoprene emissions calculated by WRF-Chem and EMEP MSC-W is very similar (Fig. 3), but there is a difference in the magnitude (Table 2) and in the horizontal distribution of the emissions (Fig. 3). The isoprene emissions calculated by WRF-Chem/MEGAN are systematically higher than that predicted by the EMEP model. These differences could be attributed to different emission factors and land use classifications. In particular, MEGAN predicts large isoprene emissions from shrublands in the western part of Turkey and southern Greece, and from broadleaf trees northwest on the Balkan Peninsula. However, the differences are well within known uncertainties, which are at least a factor of two for natural emissions (Simpson et al., 1995, 1999).

2.4 Simulations

For each model, one reference simulation and a number of sensitivity simulations have been performed in order to study the impact of different processes on surface ozone levels (Table 3). The impacts of fire emissions, biogenic emissions, anthropogenic emissions and dry deposition on ozone have been investigated by turning off the respective emission sector or process in the sensitivity simulations. In addition, as this study aims at quantifying the impact of high temperatures on surface ozone, sensitivity simulations have been performed with temperatures restricted to a maximum of 28 °C in the calculations of chemical reactions, biogenic emissions, and dry deposition. Regarding the latter simulation (MD), the Wesely (1989) scheme in WRF-Chem uses the surface skin temperature to calculate dry deposition, but the 28 °C limit has been applied to the 2 m temperature in order for the test to be comparable with the other simulations involving the 28 °C limit (MC and MB). The 28 °C limit has been chosen because it represents a typical summer temperature in the EM region. For comparison, at the National Observatory of Athens the summer (JJA) normal values (based on 1961–1990 averages) are 31.6 °C and 26.1 °C for the daily maximum and mean air temperatures, respectively (Founda and Giannakopoulos, 2009). As explained in Sect. 2.1, very high temperatures lead to closing of the plants' stomata openings and a reduction of dry deposition. According to previous literature, the emissions of isoprene from vegetation are not sensitive to stomatal closure (Niinemets et al., 2004) while another meteorological factor, soil moisture, can affect biogenic emissions (Muller et al., 2008). In the EMEP model both temperature and soil moisture affects dry deposition, while only temperature affects BVOC emissions. In WRF-Chem the dry deposition scheme takes into account changes in temperature and not soil moisture, while the BVOC emissions are affected by both temperature and soil moisture (among other meteorological factors – see Sect. 2.3).

Table 2. Emissions from various sources averaged over the region marked by the dashed line in Fig. 2 (11–30° E, 32–45° N) and for the summer period (June, July, August) of 2007, as used in the reference simulations of the two models.

	NO_x (kg(N) km^{-2} yr^{-1})	CO (kg(C) km^{-2} yr^{-1})	NMVOC (kg(NMVOC) km^{-2} yr^{-1})
WRF-Chem			
TNO-MACC anthropogenic	364.1	860.4	791.1
FINNv1 forest fires	30.9	809.1	413.7
MEGANv2 biogenic/soil	23.9	–	1918.0*
EMEP MSC-W			
Regridded EMEP anthrop.	338.2	743.7	565.3
GFEDv2 (8-day) forest fires	49.0	1233.9	387.8
EMEP biogenic/soil	–	–	949.4*

* Only isoprene emissions (kg(C_5H_8) km^{-2} yr^{-1}) given here, but note that the biogenic emission modules include also other NMVOCs such as terpenes.

Table 3. Overview of the model simulations performed by each of the two models. The WRF-Chem simulations include only gas-phase chemistry, while the EMEP MSC-W simulations include also aerosol chemistry.

Acronym	Description	WRF-Chem	EMEP MSC-W
REF	Reference (setup described in Sects. 2.1–2.3)	X	X
GF	FINN emissions replaced by GFED emissions	X[a]	
NF	No fire emissions	X	X
NB	No biogenic emissions	X	X
NA	No anthropogenic emissions	X	
ND	No dry deposition	X	
MC	Max. 28 °C for chemistry calculations in the PBL[b]	X	X
MB	Max. 28 °C when calculating biogenic emissions	X	X
MD	Max. 28 °C when calculating dry deposition	X	

[a]FINN fire emissions are used in the WRF-Chem REF simulation, but an additional WRF-Chem simulation has been done with GFED fire emissions (GF) for comparison with EMEP MSC-W simulations.
[b]Planetary Boundary Layer (PBL) taken here as the lowest 2.5 km.

3 Results and discussion

3.1 Meteorological conditions

The levels of air pollutants in the Eastern Mediterranean region are strongly affected by the unique meteorological characteristics. Etesian winds blow over the Mediterranean and are most pronounced over the Aegean Sea as northerly winds during summer (e.g. Kallos et al., 1993). The etesians are generated from large-scale dynamical systems, but are also affected by local land-sea breezes along the coast, impacting air pollution levels for instance in Athens. Air pollution in the region is further impacted by the islands and peninsulas which act as chimneys for transferring boundary layer air masses to the free troposphere, and by differential heating between North Africa, Mediterranean Sea and Southern Europe (Kallos et al., 2007, and references therein). The synoptic situation during summer 2007 is described in Founda and Giannakopoulos (2009), who attribute the heat waves to horizontal advection, downward motion causing adiabatic heating, and the preceding winter which was warm and dry in large parts of southeastern Europe (Luterbacher et al., 2007) impacting land-atmosphere interactions. The WRF-Chem output of surface temperatures and horizontal winds are given in Fig. 5 as three-day averages for each of the heat waves occurring in the EM during summer 2007. The wind fields indicate that a high pressure area is located near southern Italy in all three cases, leading to transport of dry and warm air from northern Africa towards the Balkans. Further, the etesian winds can be recognized along the Aegean Sea, most notably during the July and August heat waves. The heat wave in June was most severe in Greece, southeastern Italy and western Turkey, while the July heat wave was more widespread with daily maximum temperatures around 40 °C throughout most of the Balkan Peninsula. The August heat wave was somewhat less intense, but still the surface temperatures exceeded 35 °C in many places in the EM region. It is worth noting that both the July and August heat waves coincide with the two most destructive forest fire episodes that struck the EM area during summer 2007 (Sect. 2.3), and

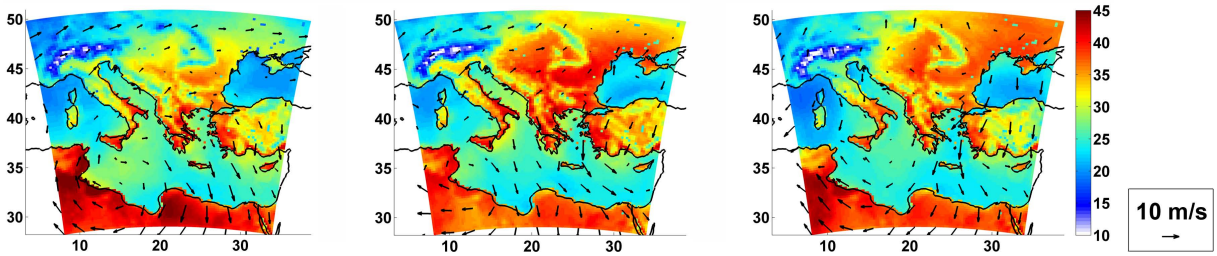

Fig. 5. Daily maximum 2 m temperature (°C) and mean 10 m wind vectors (10 m s^{-1} vector shown for scale in legend) averaged over the periods 24–26 June (left), 22–24 July (middle), and 22–24 August (right) in 2007. The winds are averaged separately in each horizontal direction (u and v wind components), and both temperature and wind averages are based on hourly output from the WRF-Chem model (i.e. 72-h averages for the winds).

this increases the potential for ozone production due to the increased emissions of ozone precursors.

3.2 Comparison with observations

The model results have been compared to ground-based measurements of ozone and satellite observations of the ozone precursors CO and NO_2. The plume from the Greek forest fires was rapidly advected towards the sea and therefore not captured by ground-based measurements. Satellite observations therefore proved to be most relevant when evaluating the modelled forest fire plumes and the forest fire emission inventories used. The comparison with ozone surface measurements is included to provide an evaluation of how the models perform with the current setup and in the extended region of interest (Table 4), although it should be noted that model validation is not the main purpose of this study.

3.2.1 CO

The Infrared Atmospheric Sounding Interferometer (IASI) onboard the MetOp-A satellite monitors the abundance of a number of atmospheric species (Clerbaux et al., 2009). CO is measured on a global scale twice a day and was shown to agree well with the retrievals of other satellite instruments (George et al., 2009). However, according to Turquety et al. (2009), who thoroughly investigated the Greek forest fire episode in August 2007, the elevated IASI CO concentrations during the 2007 fire episode were on average 35 % higher than MOPITT observations (Deeter et al., 2003).

The IASI CO columns presented here are the same as in Turquety et al. (2009), where the Fast Optimal Retrievals on Layers for IASI (FORLI) algorithm was used. When interpreting the observational data, it is important to keep in mind the sources of uncertainties, e.g. aerosol contamination, and inhomogeneities in the IASI pixels. In particular, as the IASI operational retrievals for water vapour and temperature were not available for August 2007, these profiles were taken from the ECMWF analysis data. The uncertainties are also larger in the fire plumes than in background conditions, especially close to the emissions. This means that the emphasis should be put more on a qualitative rather than a quantitative level, i.e. to identify locations for high CO rather than focusing on exact CO column values. In order to account for the different sensitivities to each vertical layer in the satellite retrievals, the model data have been weighted with IASI averaging kernels, i.e. artificial satellite retrievals were made from the model data. The IASI retrievals are performed on a 1 km vertical grid, and here we have used averages on a $0.2° \times 0.2°$ horizontal grid. For comparison, the model data were first interpolated temporally to the satellite overpass time, and spatially to the same horizontal and vertical grids. The averaging kernels were then applied to partial columns in each grid box using the formula

$$\boldsymbol{x}_{\mathrm{r}} = \boldsymbol{A} \cdot \boldsymbol{x}_{\mathrm{m}} + (\mathbf{I} - \boldsymbol{A}) \cdot \boldsymbol{x}_{\mathrm{a}} \quad (1)$$

where $\boldsymbol{x}_{\mathrm{r}}$ is the modelled satellite retrieval (molec cm^{-2}), $\boldsymbol{A}$ is the IASI averaging kernel vector for the total column, $\boldsymbol{x}_{\mathrm{m}}$ is the model data vector (molec cm^{-2}), $\mathbf{I}$ is the identity matrix, and $\boldsymbol{x}_{\mathrm{a}}$ is the IASI a priori profile (molec cm^{-2}) (Rodgers, 2000; George et al., 2009). In the comparison below, the EMEP model has been excluded because the comparison is very sensitive to processes occurring in the upper troposphere, while the EMEP model is intended for use in the lower troposphere. If a meaningful comparison was to be made, the global EMEP model (Jonson et al., 2010a, b) should have been used, but this would have put constraints on other factors important for this study (such as the horizontal resolution).

Figure 6 shows the observed and simulated total atmospheric column of CO for the intense Greek forest fire episode occurring in late August 2007. The daytime and nighttime CO columns are shown separately since the different thermal contrasts lead to large differences in the CO retrievals for day versus night (Clerbaux et al., 2009). More specifically, the temperature difference between the surface and the boundary layer over land is larger during daytime compared to nighttime, and this will lead to a higher sensitivity to the lower troposphere during the day. This difference in sensitivities is reflected in the shape of the averaging kernels and a sensible comparison with model data is

Table 4. Comparison between observed and modelled daily maximum O_3 mixing ratios (ppbv) for 10 stations (see http://ebas.nilu.no).

			Observed	WRF-Chem				EMEP MSC-W			
Station	Longitude	Latitude	Mean	Mean	Bias	RMSE	r	Mean	Bias	RMSE	r
Illmitz	16°46′ E	47°46′ N	60.1	60.7	0.6	11.0	0.68	54.5	-5.6	11.4	0.77
Payerne	6°57′ E	46°49′ N	51.5	50.9	−0.6	7.7	0.71	48.9	−2.6	8.8	0.65
Svratouch	16°3′ E	49°44′ N	48.6	54.6	6.1	9.9	0.80	51.6	3.0	9.6	0.72
Kosetice	15°5′ E	49°35′ N	52.5	53.9	1.3	8.5	0.75	49.8	−2.8	10.4	0.62
Finokalia	25°40′ E	35°19′ N	69.9	66.3	−3.4	9.2	0.36	55.4	−14.4	16.5	0.35
K-puszta	19°35′ E	46°58′ N	65.8	59.3	−6.5	9.3	0.75	55.7	−10.1	13.2	0.56
Montelibretti	12°38′ E	42°6′ N	69.5	66.1	−3.3	11.3	0.68	60.5	−9.0	14.4	0.65
Iskrba	14°52′ E	45°34′ N	58.5	56.4	−2.1	10.2	0.63	53.9	−4.6	11.5	0.56
Stara Lesna	20°17′ E	49°9′ N	54.0	52.1	−1.9	7.3	0.70	50.3	−3.7	8.4	0.63
Starina	22°16′ E	49°3′ N	54.4	54.4	0.0	13.5	0.12	49.1	−5.3	12.8	0.11
Average			58.5	57.5	−1.0	9.8	0.62	53.0	−5.5	11.7	0.56

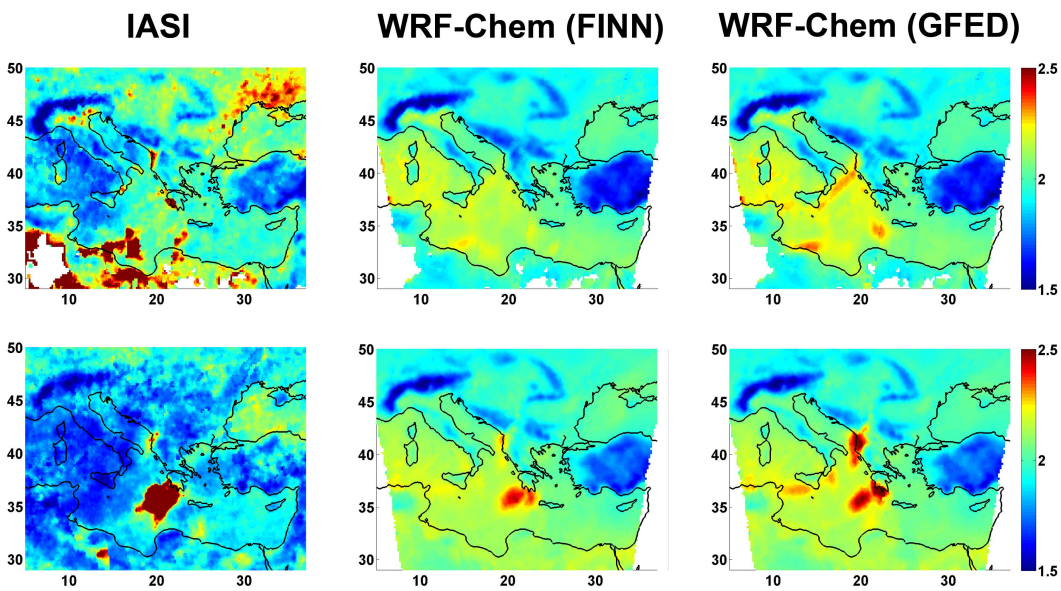

Fig. 6. Kernel weighted total columns of CO (10^{18} molec cm^{-2}) as retrieved from the IASI satellite instrument (left), and as modelled with WRF-Chem using FINN (middle) and GFED (right) forest fires emissions. The data are averaged over the period 23–28 August 2007 for daytime (top) and nighttime (bottom) retrievals. The model data have been weighted with the same averaging kernels as the IASI data.

therefore ensured. The high pressure area located over southern Italy leads to strong winds from north-northeast above Greece (Fig. 5), rapidly advecting the Greek fire plumes towards the Mediterranean Sea and the North African coast (Fig. 6). At the end of the period, the plumes mix with emissions from intense fires in Algeria, leading to enhanced CO levels over North Africa (Turquety et al., 2009). The satellite data show that forest fires in Albania and Italy also lead to CO enhancements, but the signal is weaker and the transport less efficient than for the fire plume originating from the Peloponnese fires.

The locations of the Greek forest fire plumes are reflected fairly well in the simulated retrievals, but the magnitude of the CO column in the core of the plumes is strongly underestimated by the model (Fig. 6). Also the fire plume originating from Algeria, evident in the daytime retrievals, is too low in the model results, although it should be noted that most of the Algerian forest fire emissions take place outside the WRF-Chem domain and are only taken into account through the chemical boundary conditions. The background levels of CO, however, are overestimated in the model. There are several possible reasons for the discrepancies between the model and observations. First, it should be noted that the overestimation of background CO is less pronounced when the averaging kernels were not applied (see Supplement, Fig. A1). As the sensitivity of the satellite observations is stronger at higher altitudes, the averaging kernels give more weight to the upper model layers (see Supplement, Fig. A2), and this

will cause an amplification of possible enhanced CO at these heights. Second, the comparison is also very sensitive to how the emissions are distributed vertically, and to the vertical transport in the models. If the fire emissions are implemented too close to the surface in the models, the simulated CO retrievals (modelled CO columns with averaging kernels applied) in the plume will be too low as the sensitivity of the satellite observations decreases rapidly towards the surface. As previously mentioned, about 70 % of the forest fire emissions in WRF-Chem are emitted in the lowermost layer. The diurnal profile applied to the forest fire emissions also contributes to the uncertainties, particularly because it affects how much of the emissions are in the boundary layer, which is normally more shallow during night. Other sources of uncertainty include dilution in the model grid, chemical reactivities in the model, and the uncertainties related to the observations, as previously mentioned.

Underestimation of CO fire emissions is perhaps the most important reason for the discrepancies explained above. Based on the observed and modelled fire plumes (Fig. 6), the CO emissions from forest fires seem significantly underestimated in both the inventories applied (FINN and GFED). The maximum observed CO column, which occurred on 25 August, exceeded 2.5×10^{19} molec cm^{-2}, while the corresponding model values were about one order of magnitude lower (see Supplement, Fig. A3). However, one should consider that the GFED simulation may not realistically represent maximum values due to the 8-day averaging, and that the observed CO column magnitude is uncertain due to e.g., missing operational retrievals for water vapour and temperature. Turquety et al. (2009) highlighted the large uncertainties associated with the calculation of fire emissions. They used the IASI CO burden and a bottom-up approach to estimate 30 and 41 % larger CO emissions, respectively, compared to the numbers reported in the GFED inventory for the Greek forest fires in August 2007. Also, Pfister et al. (2011) estimated that FINN emissions of CO during a forest fire episode in California in June 2008 may have been underestimated by nearly a factor 4, and they attributed this to possible errors in the MODIS land cover data, which is critical input to FINN as the land use category determines the emission factor.

3.2.2 NO_2

Modelled tropospheric columns of NO_2 have been compared to observations from the Ozone Monitoring Instrument (OMI), which is onboard the Earth Observing System Aura satellite (Levelt et al., 2006). OMI covers the globe daily with a spatial resolution of 24 km × 13 km at nadir. In this study level 2 data containing the individual pixels has been provided by IUP-Bremen using NASA NO_2 slant columns and the tropospheric column retrieval method described in Richter et al. (2005), and later gridded to a resolution of $1/16° \times 1/16°$. This data set does not provide averaging kernel information and is compared to the original vertical NO_2 column from the model. Since the tropospheric columns of NO_2 are mostly influenced by processes occurring in the lower troposphere (mainly due to strong surface emission sources and relatively short lifetime of NO_x), it was possible to include the EMEP model in this comparison.

Figure 7 shows the observed and modelled tropospheric column of NO_2 averaged over the period 21–28 August 2007. This 8-day period is chosen because it coincides both with the Greek forest fire episode and with the 8-day period in the GFED data set. As for CO, the fire plumes are clearly visible in the observations, and both models are able to capture the locations and influences of the fires. The evolution of the fire impact is much the same as for CO with northeasterly winds transporting the Peloponnese fire plume towards the Mediterranean Sea. However, the NO_2 plume is more confined to the origin of the fires due to the shorter lifetime of NO_2. The results indicate that the emissions of NO_2 from the Albanian forest fires may be overestimated in the GFED inventory as the modelled NO_2 plume with GFED data gives much higher levels than observed and also compared to the model results using FINN emissions. The large NO_2 values over Ukraine result mainly from anthropogenic emission sources and are only slightly affected by forest fire emissions during this time period. The observations show a more widespread NO_2 impact in this region, and this could indicate that a too low injection height has been used for the anthropogenic emissions, as this would cause underestimation of transport due to the rapid increase of NO_2 lifetime with altitude.

The underestimation of the Greek fire emissions seen for CO is not evident for NO_2 (Fig. 7; bottom). On the contrary, the column values in the plume modelled using GFED are now overestimated and due to the coarse spatial resolution of the emissions, the simulated plume covers a too large area. The FINN simulation yields NO_2 columns which are in the same range as the observations. This is in agreement with Pfister et al. (2011) who also found negative bias only for CO fire emissions, while other components in the FINN inventory, including NO_x, did not show such bias. As CO and NO_x are co-emitted species calculated using fixed emission factors, our results suggest that the CO/NO_x emission ratio should be re-assessed. Maximum values for the Peloponnese fires occurred on 26 August and were 1.6×10^{16}, 3.0×10^{16}, 1.8×10^{16}, and 7.7×10^{15} molec cm^{-2} for OMI, WRF-Chem with FINN, WRF-Chem with GFED, and EMEP MSC-W with GFED, respectively (see Supplement, Fig. A4). The higher maximum value in the simulation with FINN compared to GFED is not surprising as the spatial and temporal resolution is much coarser in the latter inventory, leading to emissions being smeared out over a larger area and averaged in time. The simulation with FINN emissions shows remarkably good agreement with OMI with respect to location and magnitude of the forest fire plumes (Fig. 7; bottom). Surprisingly, when comparing the GFED simulations of WRF-Chem and EMEP MSC-W, the fire plume is much less pronounced in the latter model. On the other hand, the EMEP model gives

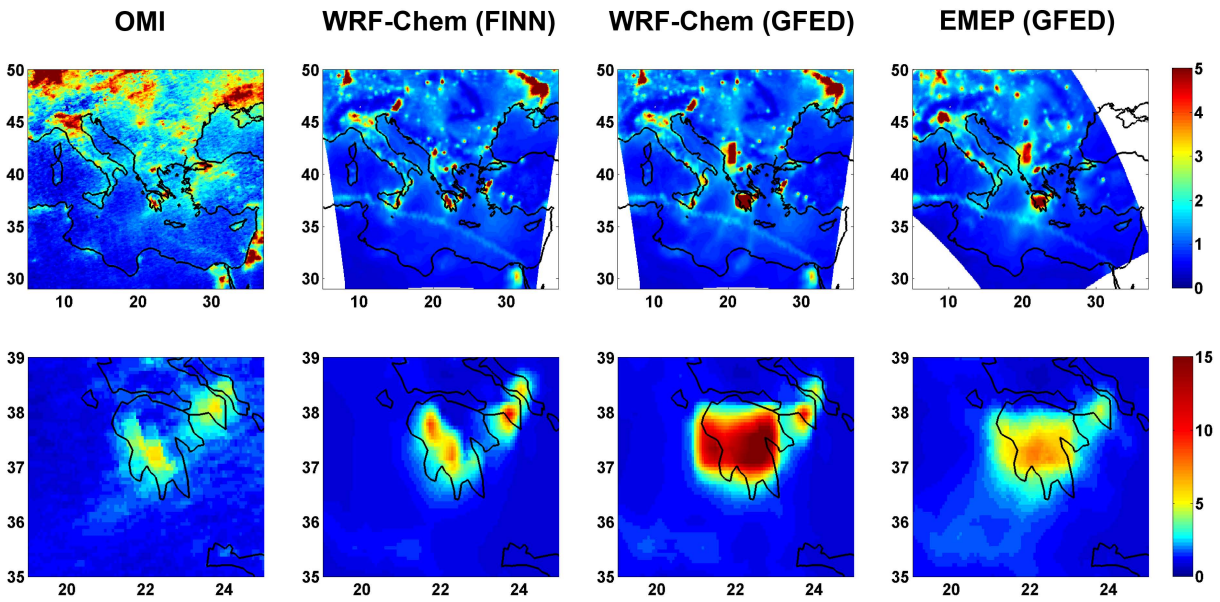

Fig. 7. Tropospheric columns of NO_2 (10^{15} molec cm^{-2}) as retrieved from the OMI satellite instrument (1st column), and as modelled with the WRF-Chem (2nd and 3rd columns) and EMEP (4th column) models, averaged over the period 21–28 August 2007 (corresponding to the 8-day period in the GFED data set). In the second column, FINN forest fire emissions have been used in the simulations, while in the two rightmost columns, GFED emissions have been used. The bottom plots have different colour scale and are zoomed in on the Peloponnese fires.

higher NO_2 levels in the plume downwind of the fires, and this is particularly evident when looking at vertical cross-sections on 26 August (see Supplement, Fig. A5), which is the day of maximum NO_2 impact from the Greek fires. This inter-model difference can mainly be explained by differences in the vertical distribution of fire emissions. Although an online plume rise routine has been applied in the WRF-Chem simulations, a much larger fraction of the forest fire emissions is placed near the surface compared to the EMEP model, which evenly distributes the emissions throughout the model's lowest eight layers (to about 1.8 km). However, other possible explanations such as differences in model dilution and reactivity of NO_x to reservoir species (e.g. HNO_3) cannot be ruled out.

The observed and modelled tropospheric columns of NO_2 (Fig. 7) reveal not only the location and influences of forest fire plumes, but a number of anthropogenic emission hotspots can also be recognized. NO_2 levels in the Po Valley tend to be underestimated by the models, while Cairo is relatively well represented in the WRF-Chem simulations (Cairo is outside the EMEP model domain). It should be noted, however, that any over- or underestimation in emissions may also be caused by the relatively crude temporal scaling factors that have been applied, and not only by potential errors in the annual numbers provided in the emission inventories. Istanbul is underestimated by both models and this is probably caused by too low emissions. A new emission inventory for the greater Istanbul area had 2–7 times higher annual emissions compared with the EMEP and TNO-MACC emissions (Im et al., 2010), mainly due to lack of officially reported emissions of Turkey to EMEP. Several other cities, including Athens, Rome and Napoli, were also captured by the observations and models, although the signal was weaker.

3.2.3 Ozone

The reference simulations of the WRF-Chem and EMEP models have been compared with ozone measurements (Hjellbrekke et al., 2011) from the 10 surface monitoring sites shown in Fig. 8 (top left). The Eastern Mediterranean region has a rather sparse selection of ground-based O_3 measurement stations categorized as rural background, which is needed for a meaningful comparison considering the model resolution used. For this reason we have extended the region for comparison to also include sites in Central and East Europe, but only those that are well within the borders of the WRF-Chem domain. The selection of stations is also based on data coverage, data quality, and geographic location (to represent as wide a region as possible). The modelled ozone values are extracted from the lowest model layer in WRF-Chem, corresponding to approximately 28 m height, while the extraction in EMEP MSC-W is based on a vertical gradient from the lowest model layer ($\sim$ 45–50 m) to 2 m height using boundary layer theory as described in Simpson et al. (2012). Previously, WRF-Chem simulations have been compared to European ground-based O_3 measurements in Zabkar et al. (2011), Hodnebrog et al. (2011) and

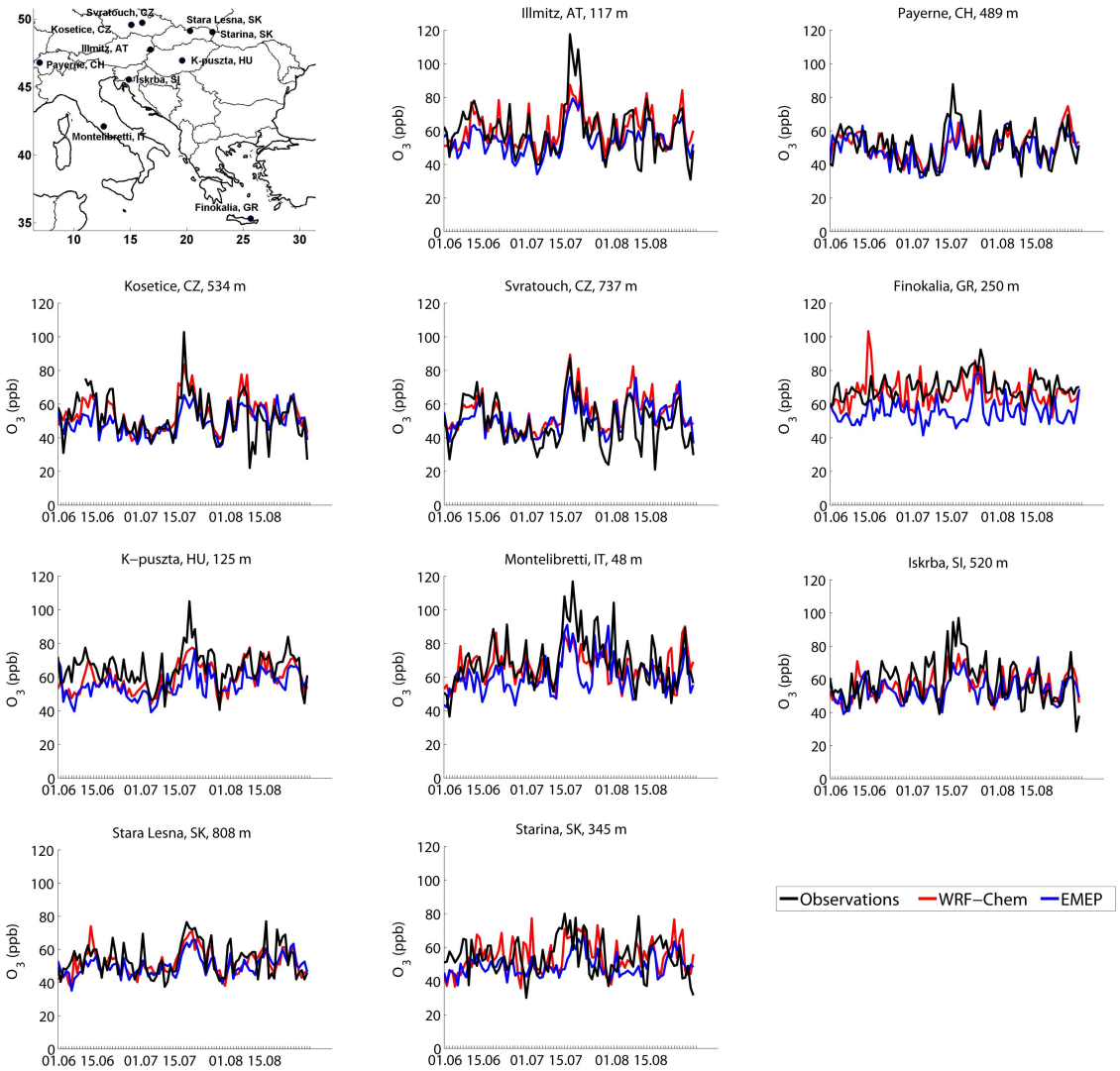

Fig. 8. Time evolution of daily maximum surface O_3 (ppbv) as measured and modelled by WRF-Chem and EMEP MSC-W for 10 stations during the summer 2007. The top left plot marks the location of each station included in the comparison.

Schürmann et al. (2009), while comprehensive validations of EMEP model results are given in the annual EMEP status reports (e.g. Gauss et al., 2011). One of the reports (Aas et al., 2010) included a special section on the Mediterranean region and pointed out the many modelling limitations in this area, with special emphasis on biogenic emissions and soil-moisture effects on stomatal exchange.

The comparisons are presented in Fig. 8 and Table 4 as time series and statistics, respectively, for daily maximum O_3 at each station and for the whole simulation period. Overall, the models perform reasonably well with an average correlation, bias and root-mean-square error (RMSE) of 0.62/0.56 (WRF-Chem/EMEP MSC-W), −1.0/−5.5 ppbv and 9.8/11.7 ppbv, respectively, but with large variations between the stations. Correlations range from around 0.1 to 0.8 and the bias is between −14 and 6 ppbv. The fact that both models have a low correlation and relatively high RMSE at the Slovakian station Starina could indicate that the measurements are influenced by local effects (e.g. biogenic emissions from nearby vegetation) which the models are not able to capture at this resolution, or there could be inaccuracies in the emission data. In general, ozone levels are slightly higher in WRF-Chem than in EMEP MSC-W, and this could be due to differences in the strength of the emissions or the different height extraction. The ozone mixing ratios based on the 2 m reduction in EMEP MSC-W is likely to be lower than the ozone values extracted from the lowest model layer due to the increasing impact of dry deposition near the surface, although this effect is less important when comparing daily maximum O_3. The negative bias in EMEP MSC-W is most notable for the Finokalia station, which is located near the coast of Crete. On the other hand, evaluation of the EMEP

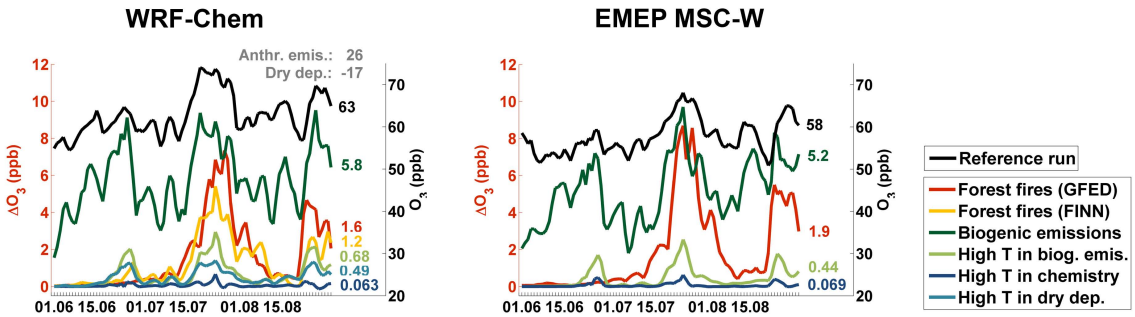

Fig. 9. Daily maximum surface ozone in the reference run (ppbv; right y-axis) and the differences between the reference run and the sensitivity runs showing the impact of various processes on daily maximum surface ozone (ppbv, left y-axis), averaged over the EM region, calculated by the WRF-Chem (left) and EMEP (right) models. Seasonally averaged values are shown next to the curves.

model for this site at other periods shows mixed results, also with overpredictions during some periods (Gauss et al., 2011). Im et al. (2011a) also had relatively large bias and only moderate correlation when comparing WRF/CMAQ model results to ozone observations at the Finokalia station, indicating that the ozone levels at this station are difficult to represent in a model at this resolution. When coarse grid resolution is used for modelling O_3 at a coastal station, such as Finokalia, the water fraction in the grid cell closest to the station may be too low, leading to overestimation of dry deposition and underestimation of ozone.

The modelled and observed ozone concentrations shown in Fig. 8 are not directly influenced by the Greek forest fire emissions due to their rapid advection towards southwest. However, the July heat wave episode seems to elevate daily maximum ozone considerably at several stations. This increase in ozone levels is well represented by the models, although with underestimation of the peak in most cases (e.g. Illmitz, Payerne, K-puszta and Iskrba). The WRF-Chem simulations reveal daily maximum temperatures reaching 35 °C and relatively calm winds in central/eastern Europe in the period 15–20 July (see Supplement, Fig. A6), and this leads to effective build-up of ozone in this area. During the following days the combination of a temperature decrease and stronger winds causes a drop in ozone concentrations, while in the southeast, on the Balkan Peninsula, an intense heat wave is established (see Sect. 3.1).

3.3 Processes impacting daily maximum O_3

In the following we present results from sensitivity studies where we have estimated the impact of various processes on the atmospheric chemistry. As the perspective of this study is air quality, we have focused on daily maximum ozone near the surface. Figure 9 shows the time evolution of daily maximum surface ozone (simulation REF), and the ozone impacts of the following processes; forest fire emissions (REF – NF and GF – NF), biogenic emissions (REF – NB), high temperatures (> 28 °C) on biogenic emissions (REF – MB), high temperatures on chemistry (REF – MC), and high temperatures on dry deposition (REF – MD), averaged over the EM region (dashed rectangle in Fig. 1). Additional sensitivity studies include ozone impacts of dry deposition (REF – ND) and anthropogenic emissions (REF – NA). The models show a similar evolution of ozone in the reference run, although the results from WRF-Chem are slightly higher than from the EMEP model throughout the summer period (averages of 63 and 58 ppbv, respectively).

Two distinctive high ozone episodes can be found in the results of both models, namely the latter half of July and the end of August (Fig. 9). The elevated O_3 concentrations in these episodes can be attributed to a combination of forest fire emissions (ΔO_3 up to 8 ppbv when averaged over the EM region), and heat waves leading to temperature-induced increases in biogenic emissions (avg. ΔO_3 up to 3 ppbv). Additionally, a sensitivity simulation with WRF-Chem (simulation MD) reveals that the high temperatures during heat waves lead to reduced dry deposition of ozone (avg. ΔO_3 up to 1.5 ppbv), and this is caused by a reduction of the plant's stomatal openings. The impact of high temperatures on chemistry, however, only led to relatively small perturbations in surface ozone (avg. ΔO_3 less than 1 ppbv) in both models. It is important to note that the numbers mentioned above are averaged over a large region, while maximum O_3 perturbations have a very inhomogeneous spatial distribution and can reach significantly higher values locally. This is shown in Table 5 which gives maximum and percentile values for each of the processes. For example the maximum O_3 impact of high temperatures on chemistry is more than two orders of magnitudes larger than the mean ozone impact. Another process, which is not quantified here, is the effect of stagnant air and thereby slower transport, often associated with heat waves. Based on the synoptic situation (Fig. 5), less advection over land may have led to increased ozone during the heat wave episodes.

During the first heat wave, occurring in late June, ozone levels were only slightly elevated. The reason is probably that forest fires only took place during the latter two heat waves

Table 5. Surface ozone mixing ratios (ppbv) in the reference run (1st row), and perturbations of surface O_3 due to various processes (rows 2–9). All values are based on model output of daily maximum surface O_3 in each gridbox the EM region for the summer 2007. Note that for dry deposition the percentiles and the maximum represent the highest negative values.

	WRF-Chem				EMEP MSC-W			
	Mean	99th percentile	99.99th percentile	Maximum	Mean	99th percentile	99.99th percentile	Maximum
Reference run	62.7	93.6	139.7	190.8	57.7	88.8	131.2	158.2
Forest fires (GFED)	1.6	23.4	90.2	157.5	1.9	23.9	69.4	94.0
Forest fires (FINN)	1.2	10.1	39.7	64.7				
Biog. emissions	5.8	19.4	37.5	55.0	5.2	17.4	38.6	63.8
High T in biog. emis.	0.7	5.0	11.6	17.7	0.5	4.2	10.5	19.4
High T in chemistry	0.1	2.3	12.4	18.8	0.1	1.4	7.7	14.3
High T in dry dep.	0.5	3.3	6.2	8.4				
Dry dep.	−16.9	−37.7	−49.8	−55.4				
Anthrop. emis.	25.7	57.0	99.2	154.9				

(except a small contribution from FINN at the end of June), and emissions from these fires caused significant ozone production (Fig. 9). However, the magnitude of forest fire impact on ozone is uncertain, with GFED emissions leading to more ozone compared to the FINN emission inventory (3-month mean ΔO_3 of 1.6 and 1.2 ppbv, respectively, when averaged over the EM region). Furthermore, GFED emissions in EMEP MSC-W caused higher ozone than GFED emissions in WRF-Chem (1.9 and 1.6 ppbv, respectively).

Figure 10 shows the spatial distribution of seasonally averaged daily maximum near-surface O_3 for the two models. The ozone distribution of both models largely reflect the distribution of precursor emissions (Fig. 2), and are also in good agreement with Poupkou et al. (2009) who studied the summer 2000 and found mean daily maximum ozone mixing ratios ranging from 65 to 95 ppbv in areas influenced by the pollution plume from Athens – mainly near the east coast of Peloponnese – and corresponding values of 65–75 ppbv near Thessaloniki. As previously mentioned, WRF-Chem gives higher surface ozone than the EMEP model, and this is more evident over sea than land. Shipping is likely a major contributor to ozone over the Mediterranean Sea, but differences in ship emissions cannot explain the differences seen between WRF-Chem and EMEP MSC-W. NO_x is the most important ozone precursor from ship emissions and the NO_x emissions from shipping used in each of the models are about the same (Fig. 2). Instead, comparison of vertical cross-sections of O_3 from the two models shows that WRF-Chem has a much stronger vertical gradient than EMEP MSC-W (see Supplement, Fig. A7). Both over land and over sea, ozone concentrations in WRF-Chem are higher than in EMEP MSC-W up to about ~ 2 km height, while the concentrations are lower above this height and up to at least 4 km. Detailed model comparison and validation is beyond the scope of this study, but we mention here a few possible reasons for the discrepancies. The chemical boundary conditions of O_3 are very different between the two models whereas WRF-Chem uses 6-hourly data from a global CTM while EMEP MSC-W is based on climatology (see Sects. 2.1 and 2.2). In addition, Table 2 shows that the emissions of ozone precursors from both anthropogenic and biogenic sources within the EM region are higher in WRF-Chem than in EMEP MSC-W, and this is likely to explain some of the differences in surface ozone. Other possible reasons include differences related to vertical mixing, chemical reaction rates and dry deposition schemes.

3.3.1 Impact of forest fires

Figure 11 shows the impact of forest fire emissions on daily maximum near-surface ozone. The uncertainties in the ozone impact are evident, and it is quite clear from these simulations that the choice of emission inventory is more important than the choice of model. In line with the differences in emissions (Fig. 2), the WRF-Chem simulation with FINN emissions yields much lower ozone impacts from the Albanian and Greek forest fires than WRF-Chem with GFED. On the other hand, fires that took place north of the Black Sea had a much stronger impact on ozone. Although maximum NO_2 columns were higher in FINN (Fig. 7), the EM maximum of summer mean daily maximum near-surface ozone concentrations (over Albania) were about three times higher with GFED (5.3 and 17.7 ppbv, respectively). The overall maximum O_3 perturbation calculated with GFED reached extremely high values, almost 160 ppbv in one grid box on August 23, compared to 65 ppbv on 24 July when using FINN emissions (Table 5). CO concentrations in this region are much smaller in the FINN simulation (Fig. 6), but this is a less probable explanation of the ozone differences as CO is relatively unreactive on these temporal and spatial scales. More likely, the higher NO_x emissions in GFED than FINN leads to increased O_3 production, but it could also be an effect of the different emission resolutions used. For this study with 25 km × 25 km model resolution, the GFED emissions (1° × 1°) are spread equally over approximately 16 grid cells, while FINN emissions (1 km × 1 km) can reproduce the model scales. The non-linear relationship between

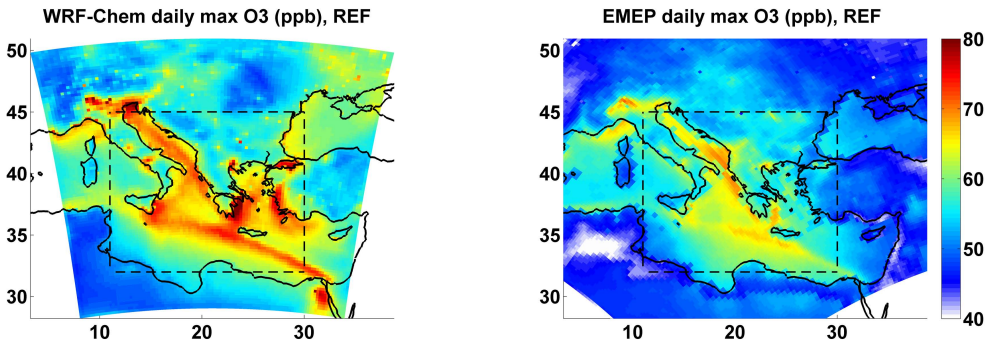

Fig. 10. Daily maximum near-surface ozone (ppbv) calculated by WRF-Chem (left) and EMEP MSC-W (right) averaged over the summer (JJA) 2007. The dashed rectangle marks the common EM region.

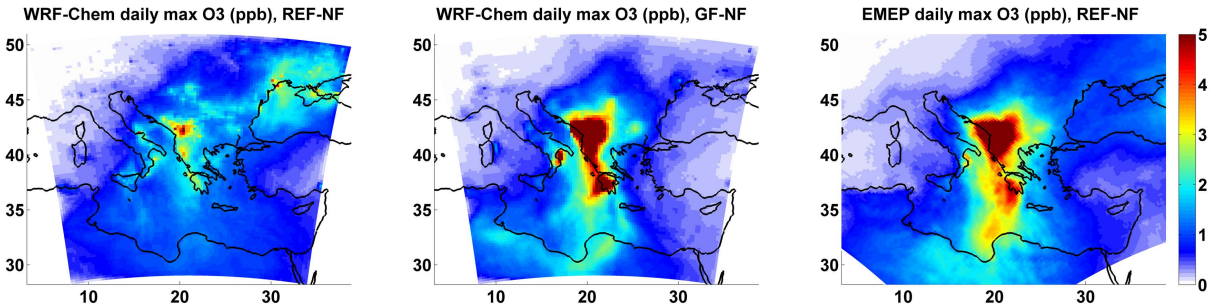

Fig. 11. Change in daily maximum near-surface ozone (ppbv) due to forest fire emissions (REF-NF and GF-NF) calculated by WRF-Chem using FINN emissions (left), WRF-Chem using GFED emissions (middle), and EMEP MSC-W using GFED emissions (right) averaged over the summer (JJA) 2007.

O_3 formation and O_3 precursors is well established (e.g. Lin et al., 1988; Kleinman et al., 2000). In a NO_x-rich emission plume, an increase in NMVOC levels will lead to more ozone production while a further increase in NO_x may lead to ozone titration through the reaction $NO + O_3$. When modelling pollution plumes, NO_x concentrations are more likely to be saturated when fine grid resolution is used, but there are competing effects which may lead to both over- and underestimation of O_3. It should also be noted that the model resolution of 25 km × 25 km used here is most likely too coarse to resolve the small-scale chemistry effects occurring within the urban and forest fire plumes. However, according to Pleim and Ching (1993), decreasing grid size does not necessarily give more realistic ozone production rates. Quantification of these sub-grid scale inaccuracies is complicated and indeed beyond the scope of this study. The reader is referred to e.g. Pleim and Ching (1993), Tie et al. (2010) and Hodnebrog et al. (2011) for a discussion of small-scale urban plume chemistry effects.

The two models yield similar impact of GFED emissions on ozone concentrations. However, in WRF-Chem the impact on ozone is more confined to the origin of the fires, leading to higher maximum values than in EMEP MSC-W (17.7 and 11.4 ppbv, respectively), while the latter model shows a more widespread ozone impact near the fires and particularly in the northeastern part of the region. The same signal was seen for the ozone precursor NO_2 (Sect. 3.2.2). Previous studies show that the two chemical mechanisms EMEP and RADM2 predict similar O_3 concentrations, except in NO_x rich environments when higher O_3 levels are predicted by EMEP (Gross and Stockwell, 2003; Jimenez et al., 2003). Hence, differences related to plume rise or meteorology in the two models are more likely to explain this feature than differences in chemistry.

3.3.2 Impact of biogenic emissions

Sensitivity simulations with both models show that the impact of biogenic emissions on daily maximum ozone is large, but very uncertain (Fig. 12). Even in the 3-months mean summer concentration, the influence of biogenic emissions is calculated to contribute significantly to daily maximum ozone; up to 10 ppbv in certain areas. The ozone impacts calculated by WRF-Chem are larger than by the EMEP model in most of the region, and reach a maximum in southwestern Turkey where impacts of about 15 ppbv are seen in WRF-Chem, while the same area in EMEP MSC-W yields less than 5 ppbv. The large impact of biogenic emissions on ozone in southwestern Turkey was also found by Im and Kanakidou (2012) who also used the MEGAN module to calculate

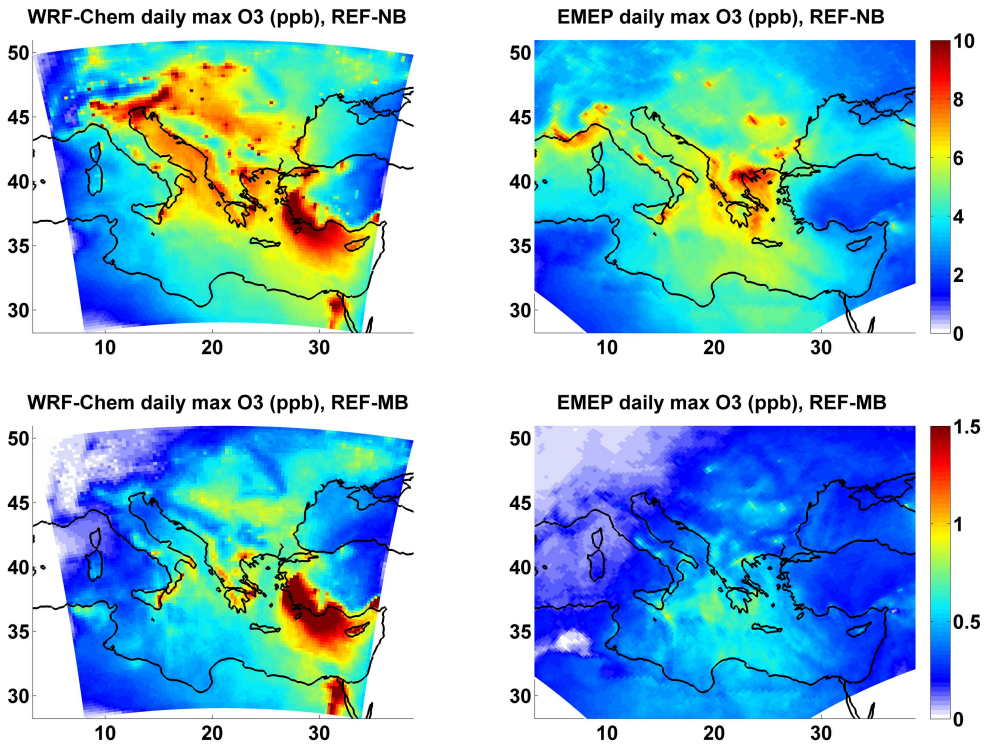

Fig. 12. Change in daily maximum near-surface ozone (ppbv) due to biogenic emissions (REF-NB) (top) and due to high temperatures (above 28 °C) in the computation of biogenic emissions (REF-MB) (bottom), calculated by WRF-Chem (left) and EMEP MSC-W (right) averaged over the summer (JJA) 2007.

biogenic emissions. On average in the EM region, the daily maximum ozone impact of biogenic emissions is 5.8 and 5.2 ppbv in WRF-Chem and EMEP MSC-W, respectively (Table 5). These differences can be attributed mainly to the differences in magnitude and distribution of biogenic isoprene emissions (Fig. 2). As mentioned in Sect. 2.3, the isoprene emissions in WRF-Chem are significantly higher than in the EMEP model, and in addition, biogenic NO emissions from soil are only included in WRF-Chem.

It is worth noting the large ozone impact of biogenic emissions over anthropogenic hotspot regions, such as the Po Valley and Cairo in WRF-Chem, and downwind of Athens in EMEP MSC-W (Fig. 12). The relatively modest biogenic emissions in these regions suggest that the large ozone impacts are not caused by biogenic emissions alone, but most probably these emissions act to increase the ozone production efficiency in regions dominated by anthropogenic emissions. Hotspot areas are often in a VOC-limited regime, and when nearby sources add biogenic emissions of VOCs, which are dominated by the very reactive isoprene gas, the ozone production may become much more efficient (Simpson, 1995). Im et al. (2011b) showed that biogenic VOC emissions intensified ozone production downwind of Istanbul.

A similar model sensitivity study keeping the temperature below 28 °C in the calculation of biogenic emissions caused a similar pattern, although much lower in magnitude (Fig. 12). Also, the distribution is more influenced by the temperature distribution (Fig. 5) with the strongest ozone impacts in regions where there is a combination of strong biogenic emissions and high temperatures, particularly in and downwind of Greece and southern Italy. In WRF-Chem the temperature effect on ozone through biogenic emissions is particularly strong in Cairo and southwestern Turkey, which are areas that are experiencing very high temperatures, while the Po Valley is only slightly affected. The difference between the two models is large, with summer mean daily maximum ozone averaged over the EM region of 0.68 and 0.43 ppbv calculated by WRF-Chem and EMEP MSC-W, respectively (Table 5), and this is due to two reasons. Firstly, the WRF-Chem biogenic emissions are larger in regions where the temperature is high, e.g. western Turkey and southern Greece. Secondly, a comparison of the daily mean 2 m temperature fields for the heat wave periods reveals that the HIRLAM meteorology used in EMEP MSC-W has lower temperatures over land compared to WRF, with differences up to 5 °C at many places (see Supplement, Fig. A8).

3.3.3 Impact of high temperatures on chemistry

The impact of increased temperatures on photo-oxidant chemistry is normally driven by several factors. As well as

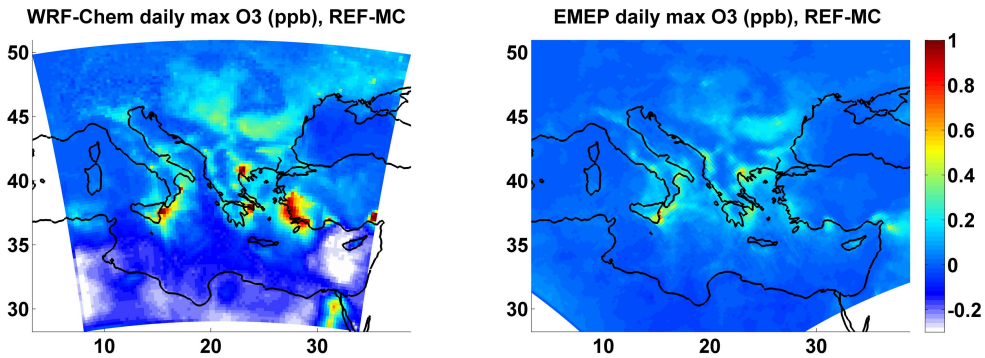

Fig. 13. Change in daily maximum near-surface ozone (ppbv) due to high temperatures (above 28 °C) in the chemistry computations (REF-MC), calculated by WRF-Chem (left) and EMEP MSC-W (right) averaged over the summer (JJA) 2007.

changing emissions of BVOC and deposition processes as already addressed, higher temperature affects many reaction rates, usually promoting ozone production. An important mechanism is that enhanced dissociation of PAN to NO_2 leads to more production of ozone (Sillman and Samson, 1995). Solberg et al. (2008) demonstrated the large impact (order of 5 %) high temperatures had on peak ozone during the European heat wave in August 2003. From Fig. 9 and Table 5 it seems that the effect of high temperatures on chemistry calculations in the EM region is relatively small with summer mean daily maximum ozone contributions of 0.063 and 0.069 ppbv calculated by the WRF-Chem and EMEP models, respectively; much lower than the ozone impact of high temperatures on biogenic emissions and dry deposition. However, there are large differences in the horizontal distribution (Fig. 13). The summer mean impact on daily maximum ozone is up to 1 ppbv in many places, particularly over large cities located in areas strongly affected by the heat waves, such as Thessaloniki and Athens. Additionally, large signals are seen near regions influenced by biogenic emissions, as e.g. southwest Turkey (in WRF-Chem), south Italy, and the northern part of the Balkan Peninsula. A small signal is also seen where the Albanian forest fires took place.

In the WRF-Chem model results, regions with slightly negative (down to −0.3 ppbv) ozone impacts of high temperatures can be seen, most notably over the Mediterranean Sea and North Africa. The reason is that high temperatures lead to faster decomposition of PAN to NO_2, and as a consequence the ozone formation will take place closer to the emission sources. As the winds come from north during the heat waves (Fig. 5), high temperatures lead to lower production of ozone south (downwind) of the major emission regions. This agrees with the findings of Sillman and Samson (1995) who suggested that ozone in the free troposphere did not increase with temperatures in the polluted PBL because the increased export of ozone, and ozone formed by exported precursors, were balanced by decreased export of PAN.

3.3.4 Impact of dry deposition

Dry deposition is the major sink for surface ozone, and contributes to a summer mean decrease in daily maximum ozone of 17 ppbv in the EM region (Table 5). The effect on daily mean concentrations would probably be even larger as dry deposition is more important during night when the PBL height is low. The horizontal distribution of the dry deposition effect on daily maximum ozone shows impacts between −20 and −30 ppbv over, and north of, the Balkan Peninsula (Fig. 14). Areas further south are more sparsely vegetated, particularly the desert in North Africa, and the impacts are therefore lower in these regions. It should be noted, however, that any ozone reduction due to dry deposition taking place outside the model domain has not been taken into account, as the lateral boundary conditions are the same in all simulations. Furthermore, the total impact of heat waves on dry deposition is probably underestimated as the Wesely (1989) dry deposition scheme used in WRF-Chem only considers changes in temperature and insolation, and not in soil moisture or near-surface humidity. The extremely low soil moisture in the summer 2007 (Founda and Giannakopoulos, 2009) is likely to have caused a significant increase in the deposition surface resistance, as highlighted by Vautard et al. (2005), Solberg et al. (2008) and Vieno et al. (2010) for the European summer 2003 heat wave.

The temperature effect on dry deposition gives increases in summer mean daily maximum ozone up to 1.5 ppbv in several places (Fig. 14). Both the magnitude and geographical distribution is similar to the temperature effect on biogenic emissions, but dry deposition has a stronger impact in the northern part of the domain. A few exceptions from the sparse vegetation in North Africa can be seen over the Nile Delta north of Cairo, and over the northern parts of Algeria and Tunisia. The temperature impact on dry deposition is relatively strong here, which is partly because these areas rather frequently experience summer temperatures above 28 °C, not only during heat wave episodes.

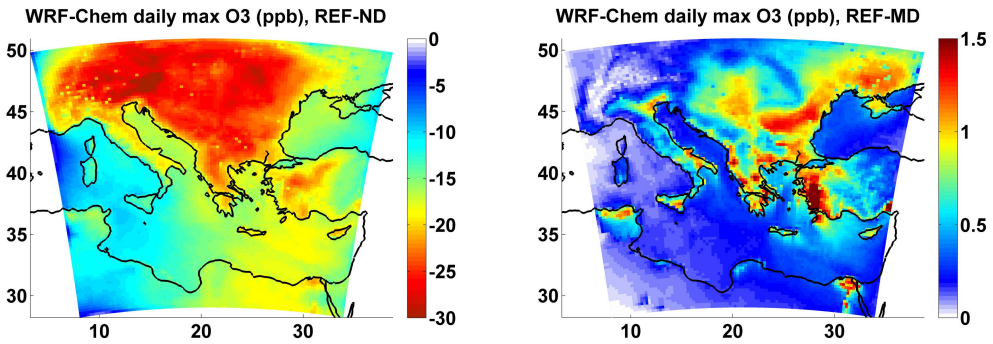

Fig. 14. Change in daily maximum near-surface ozone (ppbv) due to dry deposition (REF-ND) (left) and due to high temperatures (above 28 °C) in the computation of dry deposition (REF-MD) (right), calculated by WRF-Chem and averaged over the summer (JJA) 2007.

3.3.5 Impact of anthropogenic emissions

Ozone precursor emissions from anthropogenic sources are the single most important factor impacting ozone among the sensitivity tests studied here. In the EM region, the increase in daily max ozone concentration averaged over the summer, due to anthropogenic emissions, is 26 ppbv (Table 5), and in some regions the concentration change exceeds 45 ppbv (Fig. 15). Note that the boundary conditions are the same in all simulations, excluding impacts of anthropogenic emissions taking place outside the model domain. Thus the importance of long range transport of pollutants (e.g. O_3, NO_x, CO, HNO_3 and PAN) for the regional chemistry is different in the two simulations (REF and NA). The horizontal distribution largely follows the pattern of NO_x emissions (Fig. 2), and also the ozone fields in the reference simulation (Fig. 10). Several large cities can be recognized, but our results indicate that emissions from shipping have the strongest anthropogenic impact on ozone in the region (Fig. 15). The highest contributions are found west of Crete and north of the Nile Delta, where emissions from Athens and Cairo, respectively, mix with ship emissions and effectively produce ozone. Due to the large fraction of NO_x in ship emissions, regions near the ship tracks are usually VOC-limited, and inflow of urban pollution plumes, containing a larger fraction of VOCs, therefore leads to an increase in the ozone production efficiency. Also, as vegetation is the largest source of NMVOC in the region during summer (Table 2), additional O_3 is produced from ship emissions downwind of biogenic emissions sources. The ozone levels are further intensified by the ineffectiveness of dry deposition over sea.

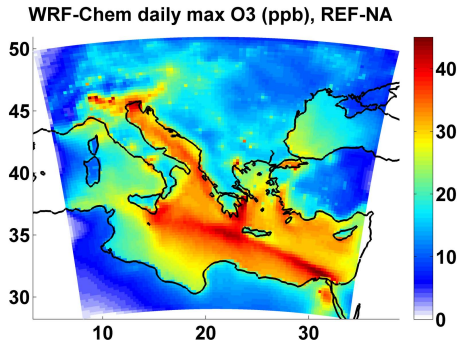

Fig. 15. Change in daily maximum near-surface ozone (ppbv) due to anthropogenic emissions (REF-NA) calculated by WRF-Chem and averaged over the summer (JJA) 2007.

4 Conclusions

Model calculations for the Eastern Mediterranean hotspot area in summer 2007 are presented using the WRF-Chem and the EMEP MSC-W models. Three heat waves and numerous wildfires struck the Eastern Mediterranean area and strongly affected air pollution levels during summer 2007. Comparisons with satellite observations of CO and NO_2 columns from IASI and OMI, respectively, show that the models are able to capture the location and influence of the fires relatively well. However, the extreme levels of CO that were observed in the Peloponnese fire plume were not reflected in the model results using WRF-Chem. This is most likely caused by underestimation of CO in the forest fire emission inventories (FINN and GFED). As the magnitude of the NO_2 fire plumes were better reflected by the models, our results suggest that the CO/NO_x fire emission ratios should be reassessed. The NO_2 comparison showed very good agreement for the simulation using FINN emissions, confirming the importance of high temporal and spatial resolution emission data. Inter-model differences were also seen, presumably caused by the different methods used for distributing the fire emissions vertically. Furthermore, the NO_2 satellite observations reveal several anthropogenic hotspots of air pollution with the Po Valley as the most dominant. The models represent the hotspot NO_2 levels relatively well, except that the tropospheric NO_2 columns over Istanbul are underestimated by at least a factor of 2 due to underestimation of emissions in this region. Model-calculated daily maximum surface O_3 concentrations are in fairly good agreement with

observations from 10 European stations. Both models and observations show elevated ozone levels in mid-July due to higher temperatures and calm winds in central/eastern Europe.

Results from sensitivity simulations show that anthropogenic emissions of ozone precursors are the largest studied contributor to daily maximum near-surface ozone concentrations in the Eastern Mediterranean during summer 2007. In some regions the summer average concentration change due to anthropogenic emissions exceeds 45 ppbv with the largest ozone perturbations located near the ship tracks. Biogenic emissions, dominated by isoprene and terpenes, react with anthropogenic NO_x emissions and contribute up to 10 ppbv ozone (3-month mean) in certain areas. However, the model differences are large with stronger ozone impact in WRF-Chem than in EMEP MSC-W, mainly because of differences in biogenic emissions. Daily maximum ozone concentrations are reduced by 20–30 ppbv in large parts of the region due to dry deposition, the major sink for surface ozone over land.

Forest fire emissions from Greece and Albania contributed substantially to ozone production, particularly in the latter half of July and the end of August. Even in the seasonal (JJA) average the models calculated forest fire impacts on daily maximum ozone up to 18 ppbv near the centre of the plume, but with large differences between the FINN and GFED emission inventories. The most intense forest fire episodes coincided with the two most severe heat waves, leading to more intense ozone production. Biogenic emissions increased as a response to high temperatures ($> 28\,^{\circ}C$), and this led to increased daily maximum ozone by up to 3 ppbv on some days when averaged over the Eastern Mediterranean region. The high temperatures also reduced dry deposition, causing up to 1.5 ppbv increase in ozone. The direct impact of high temperatures on ozone chemistry was surprisingly low (less than 1 ppbv on average over the region), because high temperatures lead to both faster O_3 production and O_3 destruction, but there were large spatial differences within the region.

Thus, if summers such as in 2007 occur more frequently in the future, ozone levels in the Eastern Mediterranean region could increase substantially due to the temperature impact on biogenic emissions and dry deposition. (Future biogenic VOC emissions will likely be affected by factors other than temperature also, e.g. CO_2 levels or soil water changes, see e.g. Arneth et al. (2007), Possell and Hewitt (2011), but such biogeochemical factors are beyond the scope of this study.) Moreover, heat wave episodes lead to increased risk of forest fires, which could further intensify ozone formation. As a consequence, these processes need to be taken into account when assessing mitigation options for the future.

Supplementary material related to this article is available online at: http://www.atmos-chem-phys.net/12/8727/2012/acp-12-8727-2012-supplement.pdf.

Acknowledgements. The research leading to these results has received funding from the European Union's Seventh Framework Programme (FP7/2007-2013) under Grant Agreement no. 212095 (CityZen) and no. 212520 (MEGAPOLI). Ø. Hodnebrog was also partly funded by the Norwegian Research Council within the project "Climate and health impacts of Short-Lived Atmospheric Components (SLAC)". A. Hilboll acknowledges funding by the Earth System Science Research School (ESSReS), an initiative of the Helmholtz Association of German research centres (HGF) at the Alfred Wegener Institute for Polar and Marine Research. OMI version-3 NO_2 slant column data was provided by NASA. We want to thank Angelika Heil, Research Center Juelich, for providing GFEDv2 emission data for various species, and Christine Wiedinmyer, National Center for Atmospheric Research, for providing the FINNv1 forest fire emissions. We would also like to acknowledge the EMEP programme for access to measurement data at http://ebas.nilu.no. NOTUR, the Norwegian metacenter for computational science, is acknowledged for giving Nilu access to the HPC (High Performance Computing) infrastructure, through the project nn9132k.

Edited by: A. Baklanov

References

Aas, W., Hjellbrekke, A., Benedictow, A., Berge, H., Fagerli, H., Gauss, M., Jonson, J. E., Nyiri, A., Simpson, D., Tsyro, S., Valdebenito, A., Shamsudheen, S. V., Wind, P., Mareckova, K., Wankmüller, R., Iversen, T., Kirkevåg, A., Seland, Ø., Haugen, J. E., and Mills, G.: Transboundary Acidification, Eutrophication and Ground Level Ozone in Europe in 2008, Norwegian Meteorological Institute, Oslo, Norway, Report 1/2010, 2010.

Andersson-Sköld, Y. and Simpson, D.: Comparison of the chemical schemes of the EMEP MSC-W and IVL photochemical trajectory models, Atmos. Environ., 33, 1111–1129, doi:10.1016/s1352-2310(98)00296-9, 1999.

Andreae, M. O. and Merlet, P.: Emission of trace gases and aerosols from biomass burning, Global Biogeochem. Cy., 15, 955–966, 2001.

Andreani-Aksoyoglu, S., Prevot, A. S. H., Baltensperger, U., Keller, J., and Dommen, J.: Modeling of formation and distribution of secondary aerosols in the Milan area (Italy), J. Geophys. Res.-Atmos., 109, D05306, doi:10.1029/2003jd004231, 2004.

Arneth, A., Miller, P. A., Scholze, M., Hickler, T., Schurgers, G., Smith, B., and Prentice, I. C.: CO_2 inhibition of global terrestrial isoprene emissions: Potential implications for atmospheric chemistry, Geophys. Res. Lett., 34, L18813, doi:10.1029/2007gl030615, 2007.

Astitha, M. and Kallos, G.: Gas-phase and aerosol chemistry interactions in South Europe and the Mediterranean region, Environ. Fluid Mech., 9, 3–22, doi:10.1007/s10652-008-9110-7, 2009.

Atkinson, R.: Atmospheric chemistry of VOCs and NO_x, Atmospheric Environment, 34, 2063–2101, doi:10.1016/s1352-2310(99)00460-4, 2000.

Baertsch-Ritter, N., Keller, J., Dommen, J., and Prevot, A. S. H.: Effects of various meteorological conditions and spatial emissionresolutions on the ozone concentration and ROG/NO_x limitationin the Milan area (I), Atmos. Chem. Phys., 4, 423–438, doi:10.5194/acp-4-423-2004, 2004.

Beniston, M.: The 2003 heat wave in Europe: A shape of things to come? An analysis based on Swiss climatological data and model simulations, Geophys. Res. Lett., 31, L02202, doi:10.1029/2003gl018857, 2004.

Benjamin, M. T., Sudol, M., Vorsatz, D., and Winer, A. M.: A spatially and temporally resolved biogenic hydrocarbon emissions inventory for the California South Coast Air Basin, Atmos. Environ., 31, 3087–3100, doi:10.1016/s1352-2310(97)00014-9, 1997.

Berge, E. and Jakobsen, H. A.: A regional scale multi-layer model for the calculation of long-term transport and deposition of air pollution in Europe, Tellus B, 50, 205–223, doi:10.1034/j.1600-0889.1998.t01-2-00001.x, 1998.

Calori, G., Finardi, S., Nanni, A., Radice, P., Riccardo, S., Bertello, A., and Pavone, F.: Long-term air quality assessment: Modeling sources contribution and scenarios in Ivrea and Torino areas, Environ. Model. Assess., 13, 329–335, doi:10.1007/s10666-007-9105-7, 2008.

Clerbaux, C., Boynard, A., Clarisse, L., George, M., Hadji-Lazaro, J., Herbin, H., Hurtmans, D., Pommier, M., Razavi, A., Turquety, S., Wespes, C., and Coheur, P.-F.: Monitoring of atmospheric composition using the thermal infrared IASI/MetOp sounder, Atmos. Chem. Phys., 9, 6041–6054, doi:10.5194/acp-9-6041-2009, 2009.

Crutzen, P. J.: Photochemical Reactions Initiated by and Influencing Ozone in Unpolluted Tropospheric Air, Tellus, 26, 47–57, 1974.

Curci, G., Beekmann, M., Vautard, R., Smiatek, G., Steinbrecher, R., Theloke, J., and Friedrich, R.: Modelling study of the impact of isoprene and terpene biogenic emissions on European ozone levels, Atmos. Environ., 43, 1444–1455, doi:10.1016/j.atmosenv.2008.02.070, 2009.

Deeter, M. N., Emmons, L. K., Francis, G. L., Edwards, D. P., Gille, J. C., Warner, J. X., Khattatov, B., Ziskin, D., Lamarque, J. F., Ho, S. P., Yudin, V., Attie, J. L., Packman, D., Chen, J., Mao, D., and Drummond, J. R.: Operational carbon monoxide retrieval algorithm and selected results for the MOPITT instrument, J. Geophys. Res.-Atmos., 108, 4399, doi:10.1029/2002jd003186, 2003.

Denier van der Gon, H. A. C., Visschedijk, A., van der Brugh, H., and Dröge, R.: A high resolution European emission data base for the year 2005, A contribution to UBA- Projekt PAREST: Particle Reduction Strategies, TNO report TNO-034-UT-2010-01895_RPT-ML, Netherlands Organisation for Applied Scientific Research, Utrecht, 2010.

Dore, C. J., Watterson, J. D., Murrells, T. P., Passant, N. R., Hobson, M. M., Choudrie, S. L., Thistlethwaite, G., Wagner, A., Jackson, J., Li, Y., Bush, T., King, K. R., Norris, J., Coleman, P. J., Walker, C., Stewart, R. A., Goodwin, J. W. L., Tsagatakis, I., Conolly, C., Downes, M. K., Brophy, N., and Hann, M. R.: UK Emissions of Air Pollutants 1970 to 2005, AEA Energy and Environment, Oxfordshire, United Kingdom, Technical Report, 2007.

Emberson, L. D., Ashmore, M. R., Simpson, D., Tuovinen, J. P., and Cambridge, H. M.: Modelling and mapping ozone deposition in Europe, Water Air Soil Pollut., 130, 577–582, doi:10.1023/a:1013851116524, 2001.

Eremenko, M., Dufour, G., Foret, G., Keim, C., Orphal, J., Beekmann, M., Bergametti, G., and Flaud, J. M.: Tropospheric ozone distributions over Europe during the heat wave in July 2007 observed from infrared nadir spectra recorded by IASI, Geophys. Res. Lett., 35, L18805, doi:10.1029/2008gl034803, 2008.

Founda, D. and Giannakopoulos, C.: The exceptionally hot summer of 2007 in Athens, Greece – A typical summer in the future climate?, Glob. Planet. Change, 67, 227–236, doi:10.1016/j.gloplacha.2009.03.013, 2009.

Freitas, S. R., Longo, K. M., Chatfield, R., Latham, D., Silva Dias, M. A. F., Andreae, M. O., Prins, E., Santos, J. C., Gielow, R., and Carvalho Jr., J. A.: Including the sub-grid scale plume rise of vegetation fires in low resolution atmospheric transport models, Atmos. Chem. Phys., 7, 3385–3398, doi:10.5194/acp-7-3385-2007, 2007.

Gauss, M., Benedictow, A. C., Fagerli, H., Steensen, B. M., and Hjellbrekke, A.: EMEP Unified model performance for acidifying and eutrophying components and photo-oxidants in 2009, Norwegian Meteorological Institute, Oslo, Norway, Report 1/2011, 2011.

George, M., Clerbaux, C., Hurtmans, D., Turquety, S., Coheur, P.-F., Pommier, M., Hadji-Lazaro, J., Edwards, D. P., Worden, H., Luo, M., Rinsland, C., and McMillan, W.: Carbon monoxide distributions from the IASI/METOP mission: evaluation with other space-borne remote sensors, Atmos. Chem. Phys., 9, 8317–8330, doi:10.5194/acp-9-8317-2009, 2009.

Gerasopoulos, E., Kouvarakis, G., Vrekoussis, M., Kanakidou, M., and Mihalopoulos, N.: Ozone variability in the marine boundary layer of the eastern Mediterranean based on 7-year observations, J. Geophys. Res.-Atmos., 110, D15309, doi:10.1029/2005jd005991, 2005.

Grell, G. A., Peckham, S. E., Schmitz, R., McKeen, S. A., Frost, G., Skamarock, W. C., and Eder, B.: Fully coupled "online" chemistry within the WRF model, Atmos. Environ., 39, 6957–6975, 2005.

Gross, A. and Stockwell, W. R.: Comparison of the EMEP, RADM2 and RACM mechanisms, J. Atmos. Chem., 44, 151–170, doi:10.1023/a:1022483412112, 2003.

Guenther, A., Karl, T., Harley, P., Wiedinmyer, C., Palmer, P. I., and Geron, C.: Estimates of global terrestrial isoprene emissions using MEGAN (Model of Emissions of Gases and Aerosols from Nature), Atmos. Chem. Phys., 6, 3181–3210, doi:10.5194/acp-6-3181-2006, 2006.

Guenther, A. B., Zimmerman, P. R., Harley, P. C., Monson, R. K., and Fall, R.: Isoprene and Monoterpene Emission Rate Variability - Model Evaluations and Sensitivity Analyses, J. Geophys. Res.-Atmos., 98, 12609–12617, doi:10.1029/93jd00527, 1993.

Hjellbrekke, A., Solberg, S., and Fjæraa, A. M.: Ozone measurements 2009, Norwegian Institute for Air Research, Kjeller, Norway, EMEP/CCC-Report 2/2011, 2011.

Hodnebrog, Ø., Stordal, F., and Berntsen, T. K.: Does the resolution of megacity emissions impact large scale ozone?, Atmos. Environ., 45, 6852–6862, doi:10.1016/j.atmosenv.2011.01.012, 2011.

Im, U. and Kanakidou, M.: Impacts of East Mediterranean megacity emissions on air quality, Atmos. Chem. Phys., 12, 6335–6355, doi:10.5194/acp-12-6335-2012, 2012.

Im, U., Markakis, K., Unal, A., Kindap, T., Poupkou, A., Incecik, S., Yenigun, O., Melas, D., Theodosi, C., and Mihalopoulos, N.: Study of a winter PM episode in Istanbul using the high resolution WRF/CMAQ modeling system, Atmos. Environ., 44, 3085–3094, doi:10.1016/j.atmosenv.2010.05.036, 2010.

Im, U., Markakis, K., Poupkou, A., Melas, D., Unal, A., Gerasopoulos, E., Daskalakis, N., Kindap, T., and Kanakidou, M.: The impact of temperature changes on summer time ozone and its pre-

cursors in the Eastern Mediterranean, Atmos. Chem. Phys., 11, 3847–3864, doi:10.5194/acp-11-3847-2011, 2011a.

Im, U., Poupkou, A., Incecik, S., Markakis, K., Kindap, T., Unal, A., Melas, D., Yenigun, O., Topcu, S., Odman, M. T., Tayanc, M., and Guler, M.: The impact of anthropogenic and biogenic emissions on surface ozone concentrations in Istanbul, Sci. Total Environ., 409, 1255–1265, doi:10.1016/j.scitotenv.2010.12.026, 2011b.

Jacob, D. J. and Winner, D. A.: Effect of climate change on air quality, Atmos. Environ., 43, 51–63, doi:10.1016/j.atmosenv.2008.09.051, 2009.

Jimenez, P., Baldasano, J. M., and Dabdub, D.: Comparison of photochemical mechanisms for air quality modeling, Atmos. Environ., 37, 4179–4194, doi:10.1016/s1352-2310(03)00567-3, 2003.

Jonson, J. E., Stohl, A., Fiore, A. M., Hess, P., Szopa, S., Wild, O., Zeng, G., Dentener, F. J., Lupu, A., Schultz, M. G., Duncan, B. N., Sudo, K., Wind, P., Schulz, M., Marmer, E., Cuvelier, C., Keating, T., Zuber, A., Valdebenito, A., Dorokhov, V., De Backer, H., Davies, J., Chen, G. H., Johnson, B., Tarasick, D. W., Stübi, R., Newchurch, M. J., von der Gathen, P., Steinbrecht, W., and Claude, H.: A multi-model analysis of vertical ozone profiles, Atmos. Chem. Phys., 10, 5759–5783, doi:10.5194/acp-10-5759-2010, 2010a.

Jonson, J. E., Valiyaveetil, S., Wind, P., Valdebenito, A., and Gauss, M.: Model validation of the global version of the EMEP Unified model, in: Development of the EMEP global modelling framework: Progress report, Joint MSC-W/MSC-E Report, EMEP/MSC-W Technical Report 1/2010, The Norwegian Meteorological Institute, Oslo, Norway, 14–31, 2010b.

Kallos, G., Kassomenos, P., and Pielke, R. A.: Synoptic and mesoscale weather conditions during air-pollution episodes in Athens, Greece, Bound.-Layer Meteor., 62, 163–184, doi:10.1007/bf00705553, 1993.

Kallos, G., Astitha, M., Katsafados, P., and Spyrou, C.: Long-range transport of anthropogenically and naturally produced particulate matter in the Mediterranean and North Atlantic: Current state of knowledge, J. Appl. Meteorol. Climatol., 46, 1230–1251, doi:10.1175/jam2530.1, 2007.

Kanakidou, M., Mihalopoulos, N., Kindap, T., Im, U., Vrekoussis, M., Gerasopoulos, E., Dermitzaki, E., Unal, A., Koçak, M., Markakis, K., Melas, D., Kouvarakis, G., Youssef, A. F., Richter, A., Hatzianastassiou, N., Hilboll, A., Ebojie, F., Wittrock, F., von Savigny, C., Burrows, J. P., Ladstaetter-Weissenmayer, A., and Moubasher, H.: Megacities as hot spots of air pollution in the East Mediterranean, Atmos. Environ., 45, 1223–1235, doi:10.1016/j.atmosenv.2010.11.048, 2011.

Kaskaoutis, D. G., Kharol, S. K., Sifakis, N., Nastos, P. T., Sharma, A. R., Badarinath, K. V. S., and Kambezidis, H. D.: Satellite monitoring of the biomass-burning aerosols during the wildfires of August 2007 in Greece: Climate implications, Atmos. Environ., 45, 716–726, doi:10.1016/j.atmosenv.2010.09.043, 2011.

Kleinman, L. I., Daum, P. H., Imre, D. G., Lee, J. H., Lee, Y. N., Nunnermacker, L. J., Springston, S. R., Weinstein-Lloyd, J., and Newman, L.: Ozone production in the New York City urban plume, J. Geophys. Res.-Atmos., 105, 14495–14511, doi:10.1029/2000jd900011, 2000.

Kourtidis, K., Zerefos, C., Rapsomanikis, S., Simeonov, V., Balis, D., Perros, P. E., Thompson, A. M., Witte, J., Calpini, B., Sharobiem, W. M., Papayannis, A., Mihalopoulos, N., and Drakou, R.: Regional levels of ozone in the troposphere over eastern Mediterranean, J. Geophys. Res.-Atmos., 107, 8140, doi:10.1029/2000jd000140, 2002.

Kuenen, J., Denier van der Gon, H. A. C., Visschedijk, A., and and van der Brugh, H.: High resolution European emission inventory for the years 2003 – 2007, TNO report TNO-060-UT-2011-00588, Utrecht, 2011.

Köble, R. and Seufert, G.: Novel Maps for Forest Tree Species in Europe, A Changing Atmosphere, 8th European Symposium on the Physico-Chemical Behaviour of Atmospheric Pollutants, Torino, Italy, 17–20 September, 2001, http://ies.jrc.ec.europa.eu/Units/cc/events/torino2001/torinocd/Documents/Terrestrial/TP35.htm, 2001.

Lazaridis, M., Spyridaki, A., Solberg, S., Smolík, J., Zdímal, V., Eleftheriadis, K., Aleksanropoulou, V., Hov, O., and Georgopoulos, P. G.: Mesoscale modeling of combined aerosol and photo-oxidant processes in the Eastern Mediterranean, Atmos. Chem. Phys., 5, 927–940, doi:10.5194/acp-5-927-2005, 2005.

Lelieveld, J., Berresheim, H., Borrmann, S., Crutzen, P. J., Dentener, F. J., Fischer, H., Feichter, J., Flatau, P. J., Heland, J., Holzinger, R., Korrmann, R., Lawrence, M. G., Levin, Z., Markowicz, K. M., Mihalopoulos, N., Minikin, A., Ramanathan, V., de Reus, M., Roelofs, G. J., Scheeren, H. A., Sciare, J., Schlager, H., Schultz, M., Siegmund, P., Steil, B., Stephanou, E. G., Stier, P., Traub, M., Warneke, C., Williams, J., and Ziereis, H.: Global air pollution crossroads over the Mediterranean, Science, 298, 5594, 794–799, doi:10.1126/science.1075457, 2002.

Levelt, P. F., Van den Oord, G. H. J., Dobber, M. R., Malkki, A., Visser, H., de Vries, J., Stammes, P., Lundell, J. O. V., and Saari, H.: The Ozone Monitoring Instrument, IEEE Trans. Geosci. Remote Sens., 44, 1093–1101, doi:10.1109/tgrs.2006.872333, 2006.

Lin, X., Trainer, M., and Liu, S. C.: On the nonlinearity of the tropospheric ozone production, J. Geophys. Res.-Atmos., 93, 15879–15888, doi:10.1029/JD093iD12p15879, 1988.

Liu, Y., Kahn, R. A., Chaloulakou, A., and Koutrakis, P.: Analysis of the impact of the forest fires in August 2007 on air quality of Athens using multi-sensor aerosol remote sensing data, meteorology and surface observations, Atmos. Environ., 43, 3310–3318, doi:10.1016/j.atmosenv.2009.04.010, 2009.

Luterbacher, J., Liniger, M. A., Menzel, A., Estrella, N., Della-Marta, P. M., Pfister, C., Rutishauser, T., and Xoplaki, E.: Exceptional European warmth of autumn 2006 and winter 2007: Historical context, the underlying dynamics, and its phenological impacts, Geophys. Res. Lett., 34, L12704, doi:10.1029/2007gl029951, 2007.

Madronich, S.: Photodissociation in the atmosphere .1. Actinic flux and the effects of ground reflections and clouds, J. Geophys. Res.-Atmos., 92, 9740–9752, 1987.

Melas, D., Ziomas, I., Klemm, O., and Zerefos, C. S.: Anatomy of the sea-breeze circulation in Athens area under weak large-scale ambient winds, Atmos. Environ., 32, 2223–2237, doi:10.1016/s1352-2310(97)00420-2, 1998.

Metzger, S., Dentener, F., Pandis, S., and Lelieveld, J.: Gas/aerosol partitioning: 1. A computationally efficient model, J. Geophys. Res.-Atmos., 107, 4312, doi:10.1029/2001jd001102, 2002.

Middleton, P., Stockwell, W. R., and Carter, W. P. L.: Aggregation and analysis of volatile organic-compound emissions for

regional modeling, Atmos. Environ. Part A, 24, 1107–1133, doi:10.1016/0960-1686(90)90077-z, 1990.

Millan, M. M., Salvador, R., Mantilla, E., and Kallos, G.: Photooxidant dynamics in the Mediterranean basin in summer: Results from European research projects, J. Geophys. Res.-Atmos., 102, 8811–8823, doi:10.1029/96jd03610, 1997.

Millan, M. M., Mantilla, E., Salvador, R., Carratala, A., Sanz, M. J., Alonso, L., Gangoiti, G., and Navazo, M.: Ozone cycles in the western Mediterranean basin: Interpretation of monitoring data in complex coastal terrain, J. Appl. Meteorol., 39, 487–508, doi:10.1175/1520-0450(2000)039<0487:ocitwm>2.0.co;2, 2000.

Millan, M. M., Sanz, M. J., Salvador, R., and Mantilla, E.: Atmospheric dynamics and ozone cycles related to nitrogen deposition in the western Mediterranean, Environ. Pollut., 118, 167–186, doi:10.1016/s0269-7491(01)00311-6, 2002.

Müller, J.-F., Stavrakou, T., Wallens, S., De Smedt, I., Van Roozendael, M., Potosnak, M. J., Rinne, J., Munger, B., Goldstein, A., and Guenther, A. B.: Global isoprene emissions estimated using MEGAN, ECMWF analyses and a detailed canopy environment model, Atmos. Chem. Phys., 8, 1329–1341, doi:10.5194/acp-8-1329-2008, 2008.

Niinemets, U., Loreto, F., and Reichstein, M.: Physiological and physicochemical controls on foliar volatile organic compound emissions, Trends Plant Sci., 9, 180–186, doi:10.1016/j.tplants.2004.02.006, 2004.

Pfister, G. G., Avise, J., Wiedinmyer, C., Edwards, D. P., Emmons, L. K., Diskin, G. D., Podolske, J., and Wisthaler, A.: CO source contribution analysis for California during ARCTAS-CARB, Atmos. Chem. Phys., 11, 7515–7532, doi:10.5194/acp-11-7515-2011, 2011.

Pleim, J. E. and Ching, J. K. S.: Interpretive analysis of observed and modeled mesoscale ozone photochemistry in areas with numerous point sources, Atmos. Environ. Part A, 27, 999–1017, doi:10.1016/0960-1686(93)90013-o, 1993.

Possell, M. and Hewitt, C. N.: Isoprene emissions from plants are mediated by atmospheric CO_2 concentrations, Glob. Change Biol., 17, 1595–1610, doi:10.1111/j.1365-2486.2010.02306.x, 2011.

Poupkou, A., Symeonidis, P., Lisaridis, I., Melas, D., Ziomas, I., Yay, O. D., and Balis, D.: Effects of anthropogenic emission sources on maximum ozone concentrations over Greece, Atmos. Res., 89, 374–381, doi:10.1016/j.atmosres.2008.03.009, 2008.

Poupkou, A., Melas, D., Ziomas, I., Symeonidis, P., Lisaridis, I., Gerasopoulos, E., and Zerefos, C.: Simulated Summertime Regional Ground-Level Ozone Concentrations over Greece, Water Air Soil Pollut., 196, 169–181, doi:10.1007/s11270-008-9766-0, 2009.

RETRO: REanalysis of the TROpospheric chemical composition over the past 40 years, http://retro.enes.org (last access: March 2012), 2006.

Richter, A., Burrows, J. P., Nuss, H., Granier, C., and Niemeier, U.: Increase in tropospheric nitrogen dioxide over China observed from space, Nature, 437, 129–132, doi:10.1038/nature04092, 2005.

Rodgers, C. D.: Inverse methods for atmospheric sounding: theory and practice, Atmos. Ocean. Planet. Phys., 2, 238 pp., World Scientific, River Edge, NJ, 2000.

Schürmann, G. J., Algieri, A., Hedgecock, I. M., Manna, G., Pirrone, N., and Sprovieri, F.: Modelling local and synoptic scale influences on ozone concentrations in a topographically complex region of Southern Italy, Atmos. Environ., 43, 4424–4434, doi:10.1016/j.atmosenv.2009.06.017, 2009.

Schär, C., Vidale, P. L., Luthi, D., Frei, C., Haberli, C., Liniger, M. A., and Appenzeller, C.: The role of increasing temperature variability in European summer heatwaves, Nature, 427, 332–336, doi:10.1038/nature02300, 2004.

Sillman, S. and Samson, F. J.: Impact of Temperature on Oxidant Photochemistry in Urban, Polluted Rural and Remote Environments, J. Geophys. Res.-Atmos., 100, 11497–11508, doi:10.1029/94jd02146, 1995.

Simpson, D.: Biogenic Emissions in Europe .2. Implications for Ozone Control Strategies, J. Geophys. Res.-Atmos., 100, 22891–22906, doi:10.1029/95jd01878, 1995.

Simpson, D., Guenther, A., Hewitt, C. N., and Steinbrecher, R.: Biogenic emissions in Europe .1. Estimates and uncertainties, J. Geophys. Res.-Atmos., 100, 22875–22890, 1995.

Simpson, D., Winiwarter, W., Borjesson, G., Cinderby, S., Ferreiro, A., Guenther, A., Hewitt, C. N., Janson, R., Khalil, M. A. K., Owen, S., Pierce, T. E., Puxbaum, H., Shearer, M., Skiba, U., Steinbrecher, R., Tarrason, L., and Oquist, M. G.: Inventorying emissions from nature in Europe, J. Geophys. Res.-Atmos., 104, 8113–8152, 1999.

Simpson, D., Tuovinen, J. P., Emberson, L., and Ashmore, M. R.: Characteristics of an ozone deposition module II: Sensitivity analysis, Water Air Soil Pollut., 143, 123–137, doi:10.1023/a:1022890603066, 2003.

Simpson, D., Benedictow, A., Berge, H., Bergström, R., Emberson, L. D., Fagerli, H., Flechard, C. R., Hayman, G. D., Gauss, M., Jonson, J. E., Jenkin, M. E., Nyíri, A., Richter, C., Semeena, V. S., Tsyro, S., Tuovinen, J.-P., Valdebenito, Á., and Wind, P.: The EMEP MSC-W chemical transport model – technical description, Atmos. Chem. Phys., 12, 7825–7865, doi:10.5194/acp-12-7825-2012, 2012.

Skamarock, W. C. and Klemp, J. B.: A time-split nonhydrostatic atmospheric model for weather research and forecasting applications, J. Comput. Phys., 227, 3465–3485, doi:10.1016/j.jcp.2007.01.037, 2008.

Sofiev, M., Vankevich, R., Lotjonen, M., Prank, M., Petukhov, V., Ermakova, T., Koskinen, J., and Kukkonen, J.: An operational system for the assimilation of the satellite information on wildland fires for the needs of air quality modelling and forecasting, Atmos. Chem. Phys., 9, 6833–6847, doi:10.5194/acp-9-6833-2009, 2009.

Solberg, S., Hov, Ø., Sovde, A., Isaksen, I. S. A., Coddeville, P., De Backer, H., Forster, C., Orsolini, Y., and Uhse, K.: European surface ozone in the extreme summer 2003, J. Geophys. Res.-Atmos., 113, D07307, doi:10.1029/2007jd009098, 2008.

Stockwell, W. R., Middleton, P., Chang, J. S., and Tang, X. Y.: The 2nd generation regional acid deposition model chemical mechanism for regional air-quality modeling, J. Geophys. Res.-Atmos., 95, 16343–16367, 1990.

Symeonidis, P., Poupkou, A., Gkantou, A., Melas, D., Yay, O. D., Pouspourika, E., and Balis, D.: Development of a computational system for estimating biogenic NMVOCs emissions based on GIS technology, Atmos. Environ., 42, 1777–1789, doi:10.1016/j.atmosenv.2007.11.019, 2008.

Søvde, O. A., Gauss, M., Smyshlyaev, S. P., and Isaksen, I. S. A.: Evaluation of the chemical transport model Oslo CTM2 with focus on arctic winter ozone depletion, J. Geophys. Res.-Atmos., 113, D09304, doi:10.1029/2007jd009240, 2008.

Tie, X., Brasseur, G., and Ying, Z.: Impact of model resolution on chemical ozone formation in Mexico City: application of the WRF-Chem model, Atmos. Chem. Phys., 10, 8983–8995, doi:10.5194/acp-10-8983-2010, 2010.

Turquety, S., Hurtmans, D., Hadji-Lazaro, J., Coheur, P.-F., Clerbaux, C., Josset, D., and Tsamalis, C.: Tracking the emission and transport of pollution from wildfires using the IASI CO retrievals: analysis of the summer 2007 Greek fires, Atmos. Chem. Phys., 9, 4897–4913, doi:10.5194/acp-9-4897-2009, 2009.

van der Werf, G. R., Randerson, J. T., Giglio, L., Collatz, G. J., Kasibhatla, P. S., and Arellano Jr., A. F.: Interannual variability in global biomass burning emissions from 1997 to 2004, Atmos. Chem. Phys., 6, 3423–3441, doi:10.5194/acp-6-3423-2006, 2006.

Vautard, R., Honore, C., Beekmann, M., and Rouil, L.: Simulation of ozone during the August 2003 heat wave and emission control scenarios, Atmos. Environ., 39, 2957–2967, doi:10.1016/j.atmosenv.2005.01.039, 2005.

Vieno, M., Dore, A. J., Stevenson, D. S., Doherty, R., Heal, M. R., Reis, S., Hallsworth, S., Tarrason, L., Wind, P., Fowler, D., Simpson, D., and Sutton, M. A.: Modelling surface ozone during the 2003 heat-wave in the UK, Atmos. Chem. Phys., 10, 7963–7978, doi:10.5194/acp-10-7963-2010, 2010.

Visschedijk, A. J. H., Zandveld, P. Y. J., and Denier van der Gon, H. A. C.: A High Resolution Gridded European Emission Database for the EU Integrate Project GEMS, TNO report 2007-A-R0233/B, 2007.

Wesely, M. L.: Parameterization of surface resistances to gaseous dry deposition in regional-scale numerical-models, Atmos. Environ., 23, 1293–1304, 1989.

Wiedinmyer, C., Akagi, S. K., Yokelson, R. J., Emmons, L. K., Al-Saadi, J. A., Orlando, J. J., and Soja, A. J.: The Fire INventory from NCAR (FINN): a high resolution global model to estimate the emissions from open burning, Geosci. Model Dev., 4, 625–641, doi:10.5194/gmd-4-625-2011, 2011.

(Western Regional Air Partnership): 2002 Fire Emission Inventory for the WRAP Region- Phase II, Project No. 178-6, available at: http://www.wrapair.org/forums/fejf/tasks/FEJFtask7PhaseII.html (last access: 27 July 2011), 2005.

Zabkar, R., Rakovec, J., and Koracin, D.: The roles of regional accumulation and advection of ozone during high ozone episodes in Slovenia: A WRF/Chem modelling study, Atmos. Environ., 45, 1192–1202, doi:10.1016/j.atmosenv.2010.08.021, 2011.